## AD NUMBER

AD517147

## CLASSIFICATION CHANGES

TO: unclassified

FROM: confidential

## LIMITATION CHANGES

TO:

Approved for public release, distribution unlimited

FROM:

Distribution limited to U.S. Gov't. agencies only; Test and Evaluation; Jul 71. Other requests for this document must be referred to Director, Naval Research Lab., Washington, D.C. 20390. NOFORN.

## AUTHORITY

NRL ltr, 22 Aug 2002; NRL ltr, 22 Aug 2002

## AD NUMBER

**AD517147**

## CLASSIFICATION CHANGES

TO

**confidential**

FROM

**secret**

## AUTHORITY

**31 Jul 1983, per document marking, DoDD 5200.10**

NRL Memorandum Report 2297
Copy No. [redacted] of [redacted] Copies



# F-4B and F-8 Flare Effectiveness Against the ATOLL Missile (AA-2)

[Unclassified Title]

H. Toothman and C. Loughmiller

*Airborne Radar Branch*
*Radar Division*

July 1971



SPECIAL HANDLING REQUIRED
NOT RELEASABLE TO FOREIGN NATIONALS



NAVAL RESEARCH LABORATORY
Washington, D.C.

**SECURITY**

This document contains information affecting the national defense of the United States within the meaning of the Espionage Laws, Title 18, U.S.C., Sections 793 and 794. The transmission or revelation of its contents in any manner to an unauthorized person is prohibited by law.

SECRET

Memorandum

Subject: F-4B and F-8 Flare Effectiveness Against the ATOLL Missile (AA-2)

## Background

(S) The ATOLL is the most frequently observed air-to-air missile in Communist controlled countries such as North Vietnam. It is an accurate copy of the early Sidewinder and data which permit its accurate simulation are readily available. Previous studies have indicated the limited effectiveness of aircraft maneuver as a countermeasure. This study is an extension of an effort to find effective countermeasures against ATOLL.

## Findings

(S) Existing infrared flares have substantial ATOLL countermeasure capability. The primary effectiveness of the flare lies in developing large miss distances, although a significant part of its effectiveness is due to early detonation of the warhead by the infrared activated fuze.

(S) Some areas of ATOLL capability remain despite the use of the flare.

## R&D Implications

(S) The flare considered in this study was generally but not invariably effective. Further study is needed to completely determine the effectiveness of flares in realistic tactical situations. Since, in most cases, the effectiveness of the flare depended upon the timing of its ejection, enemy aircraft and/or missile detectors will be required. Parametric studies of flare luminosity, burn time, luminosity-time variations, ejection direction, ejection velocity, and flare drag variations could yield design information for significantly more effective flares.

## Recommended Action

(S) Studies of luminosity time history modification and drag reduction should be pursued in order to optimize flares within space and weight limitations. An investigation of the requirements for attack sensing and flare control should also be initiated.

Clair M. Loughmiller
Head, Tactical Analysis Section
Airborne Radar Branch



SECRET

## Table of Contents

(Unclassified)

## Abstract

(Secret)

The effectiveness of flares as a countermeasure for the ATOLL missile was investigated for the F-4B and F-8 aircraft. Many different flare ejection times for each value of missile launch range, launch aspect angle, target maneuver, and ejection direction were examined by digital simulation. Although in most cases the flare effectively counters the ATOLL, many cases required that the flare, to be effective, had to be ejected within a narrow time interval.


## Problem Status

(Unclassified)

This is a final report on flare effectiveness. Work on other countermeasures is continuing.

## Authorization

NRL Problem 53D01-03

A05-5333647/652-1/53190000

A05-536-318/652-1/W3312-00-00

## I. Introduction

(S) This study is part of a larger effort to determine the effectiveness of and the requirements for countermeasures to the ATOLL missile (AA-2). Two earlier reports (1, 2) deal with the effectiveness of maneuvers by the F-4B and F-8 aircraft as countermeasures to the ATOLL. Since maneuver alone was found to be only partly effective, flares were selected as the next most readily available technique to defeat ATOLL.

(S) The introduction of the flare into the overall study required several additions to the computer simulation used to evaluate ATOLL performance. Besides addition of the dynamic and luminosity characteristics of the flare, the missile seeker model had to be revised to handle the second "target" (flare). The passive infrared fuze of the ATOLL also required that the simulation include the possibility of the flare actuating the fuze before the missile reached the target. These additions and modifications to the simulation are described below.

## II. Simulation

### A. General Description

(U) The simulation is a 5-degree-of-freedom force and moment model of the ATOLL missile. Beginning with the initial missile/target kinematics, tracking error and proportional navigational commands are calculated. The navigational commands are used as inputs to calculate the response of the torque servo-command system. Canard deflection and the dynamic conditions of the missile are the basis for the calculation of the pitch and yaw torques, and the normal and longitudinal forces. These torques and forces are integrated to determine the missile trajectory. This mathematical model is described in detail in (1) except for the two-target/seeker model which is described later in this report.

(U) The ATOLL targets (U.S. aircraft) are modeled more simply. Their maneuver response is simulated by an $80^{\circ}$/sec roll rate and a one-second ramp to change lift. Thrust and drag are calculated to provide realistic slowdown characteristics. A maximum lift coefficient curve is used to determine maneuver limits. The aerodynamic and infrared characteristics of the F-4B and F-8 aircraft used for this study are found in (1, 2).

(U) The flare is modeled by assigning to it a drag coefficient, an initial position, and a velocity which are then integrated to provide its trajectory. The flare radiant intensity is a function of altitude, speed, and time after launch. The detailed description of the flare follows.

B. Flare Model

1. Aerodynamics

(U) The flare modeled in this study is intended to be similar to the MK 46. However, very early data on the MK 46 were used, so the characteristics may not be a good description of that flare.

(C) Since the conventional flare has no thrust, its only significant aerodynamic characteristic is drag. This drag is quite complex, however, because of the asymmetry, lack of stabilization, size and mass changes, and the burning process. Since theoretical calculation seemed impracticable, a simple empirical idea was used. The terminal velocity of the MK 46 at 10,000 ft altitude was observed to be about 100 ft/sec. Since the gravitational force equals the drag at terminal velocity,

$$mg = 1/2\rho v_f^2 s C_D \qquad 1)$$

where m is the mass of the flare, g is the acceleration due to gravity, $\rho$ is the air density, $v_f$ is the speed of the flare, s is the reference area of the flare, and $C_D$ is the drag coefficient of the flare. After substituting for the observed terminal velocity and transposing, Eq. 1 becomes:

$$\frac{s C_D}{m} = \frac{2g}{v_f^2} = 3.67 \text{ ft}^2/\text{slug} \qquad 2)$$

Equation 2 is sufficient to describe the trajectory of the flare using Newton's Laws of Motion. Figure 1 shows some sample results using this approach.

(C) Since the simulation keeps track of the position, velocity, and orientation of the target aircraft, and the location of the ALE-29 flare dispenser is known, it is possible to calculate the trajectory of the flare. It is assumed that the flare is ejected at 80 ft/sec.

(C) Two ALE-29's are located on each side of the F4-B near the tail as shown in Fig. 2. They eject flares somewhat above the horizontal of the aircraft. The ALE-29 on the F-8, shown in Fig. 3, ejects the flare downward from the aircraft.

2. Radiant Intensity and Size

(S) The radiant intensity of a flare is a function of its ignition delay, altitude, and speed. As shown in Fig. 4, the simulation provides a nominal ignition delay of 100 ms after ejection.

The static radiant intensity of the flare in the ATOLL bandpass is assumed to be 900 watts/str at 10 K ft altitude and 600 watts/str at 35 K ft. A linear extrapolation is used for other altitudes.

(C) The effects of speed on flare radiant intensity were developed in a somewhat arbitrary manner, but have proven to be a fair approximation of reality (3). The equation used is

$$\text{Radiant intensity} = (\text{static radiant intensity } 1 - \left(\frac{v_f - 100}{v_f}\right)$$

Radiant intensity as a function of time and altitude is shown on Fig. 4.

(C) The angular size of a target is an important factor in determining the tracking signal in the ATOLL seeker. It is second in importance only to the radiant intensity of the flare. Motion pictures of a burning MK 46 led to the estimate that the effective diameter of the flare is one foot. The effects of target size upon the seeker are included in the following description of the two-target/seeker model.

## C. Two-Target Seeker Model

### 1. Introduction

(U) The ATOLL seeker model explained in (C) was based on measured values of seeker tracking rate as a function of tracking error for a single source. After consideration of the manner in which the ATOLL's checkerboard reticle develops tracking information, it becomes clear this model cannot be extrapolated to multi-target situations. The natural assumption that the seeker will track some center of radiant intensity is seen to be incorrect from the following observation. When two targets of equal radiant intensity fall into two adjacent annuli of the reticle, as shown in Fig. 5, they produce no net signal on the photocell as the reticle spins and therefore no tracking signal. The seeker model which follows accounts for such situations and also the effects of target size.

### 2. Image size

(S) The image size of a target on the ATOLL reticle is a function of the target size, the range, and the tracking error of the seeker. The apparent angular size of the target produces a proportionally sized image. However, spherical aberration in the seeker produces a minimum size image whose size increases as tracking error increases. Since the optics collimate at infinity, the image of a target at a finite range is spread due to focusing off the plane of the reticle.

The formula used for the image size, developed for the Sidewinder 1A (AIM-9B) in (4), was simplified by taking the image shape to be circular rather than elliptical. Similarly, the target shape was simplified to be a circle with the same area as the projected target tailpipe. Generally, a tailpipe appears to be elliptical, but at realistic attack angles off the tail it may be assumed to be circular. The formula for image size becomes

$$a_I = 0.00247 + 0.052\epsilon + 7.683\epsilon^2 + \frac{rf_e}{R} + \frac{0.46\ f_e^2}{R - f_e}$$

where $a_I$ is the image radius in inches, $\epsilon$ is the tracking error in radians, r is the object radius in inches, R is the object range in inches and $f_e$ is the ATOLL focal length in inches.

3. Radial Modulation Efficiency

(U) When an image lies in more than one annulus of the reticle "checkerboard," the energy in one annulus produces a signal which cancels some of the signal from an adjacent annulus. This feature was designed to reduce the effect of large objects, such as clouds, by arranging to cancel most of the energy from these large objects. Thus, to find the net tracking signal caused by a target, the various cancellations must be calculated. To facilitate computations, it is assumed that the image energy is uniformly distributed along the diameter of the image which, if extended, would go through the center of the reticle as shown in Fig. 6.

(C) Looking at Fig. 6, and assuming a uniform distribution of energy along the image diameter, the fraction of the total energy which produces the net photocell signal may be found by alternately adding and subtracting the energy in the segments of the annuli. This value, when divided by the total diameter, gives F, the radial efficiency factor,

$$F = \frac{\left| \sum_{n=1}^{15} (-1)^n d_n \right|}{2\ a_I}, \qquad 3)$$

where $d_n$ is the image diameter segment in annulus n. There are 15 modulation annuli on the ATOLL reticle. Any part of the image which falls off the reticle is ignored in the numerator of Eq. 3 but not in the denominator. Similarly, any part of the image which lies in the semicircle of the reticle opposite the image center (i.e., any part of

the image diameter on the opposite side of the reticle center from the image center) is also ignored in the numerator but included in the denominator. Later the sign of the numerator of Eq. 3 (before the absolute value is taken) is used to determine the interference effects of 2 targets.

4. Sector Modulation Efficiency

(U) Just as large images spread over more than one annulus and lose tracking effectiveness thereby, so also do they lose effectiveness by spreading over more than one sector of the reticle. Looking at the larger image in Fig. 7A, it is clear that at all times a significant part of this image is prevented from reaching the photocell. On the assumption that the sectors are rectangles, the large target of Fig. 7A produces a peak energy through the reticle of 61% of its total energy. In contrast, if the same energy were concentrated in the small target of Fig. 7A, 100% of the peak energy would reach the reticle over a substantial part of the reticle chopping cycle. Thus a sector efficiency factor, E, is used in the simulation to determine the tracking effectiveness of each image.

(S) A formula, given in (4) for images which cover up to one sector width in radius (e.g., large image in Fig. 7A), has been extrapolated to allow for any target size.

$$E = (1.0 - 0.0858R_{m2} - 0.207R_{m2}^{2}) \frac{R_{m2}}{R_m} , \qquad 4)$$

where

$$R_{m2} = R_m \text{ modulo } 2$$

and

$$R_m = \frac{2a_I}{\delta_s \epsilon f_e}$$

where $R_m$ is the diameter of the image in sector widths and $\delta_s$ is the angular width of the sectors in radians. A plot of E as a function of $R_m$ is given in Fig. 7B. The approximation for $R_m$ is consistent with the other approximations made in the seeker model and breaks down only for large targets near the center of the reticle.

(U) It may be noted that in Eq. 4, $E = 0$ for $R_m = 2$, whereas intuitive analysis of the large image Fig. 7A leads to $E > 0$. Thus Eq. 4 is conservative when $R_m$ is near 2, 4, 6, etc.

## 5. Two-Target Interactions

(U) The usual multi-target tracking model assumes that the seeker will track the center of energy of the targets. This simulation does so also, but only after the targets' signals have been modified to account for the mutual interference of the target signals in the seeker photocell. An infrared target in the ATOLL field of view is transformed by the spinning reticle and photocell into an alternating electrical signal having 6 cycles during half of the reticle spin cycle and into d.c. for the other half of the cycle. In general, when two or more targets are present, the 6 cycle modulations of the targets will overlap and interfere as shown in Fig. 8. The loss of signal in the overlap zone and the duration of the overlap can be calculated to provide a basis for assigning effective target center angles as well as effective target amplitudes.

(C) First it is necessary to calculate the extent of the interference in the overlap zone. The target modulations produced by the reticle are not necessarily sinusoidal. They more often resemble a square wave (i.e., small and/or distant target). For this reason (and for simplicity), Eq. 5 is based on square waves. The "weight," $W_I$, of each target is

$$W_I = \frac{S_1 E_1 F_1}{S_1 E_1 F_1 + S_2 E_2 F_2 + N} \qquad 5)$$

where N is the noise power and the subscripts refer to the two targets. The weight, $W_I$, in the overlap zone is given by

$$W_I = \left| W_1 + n_1 n_2 W_2 \right| \frac{\delta - \Delta}{\delta} + \left| W_1 - n_1 n_2 W_2 \right| \frac{\Delta}{\delta}$$

where $n_1$ equals $\pm 1$ depending on whether the numerator of $F_1$ is positive or negative, $\delta$ is the angle of a modulation sector ($\delta = \pi/12$), and the relative phase of the two square waves,

$$\Delta = \left| (\phi_{\epsilon_1} - \phi_{\epsilon_2}) \bmod \delta \right| .$$

(C) With $W_1$, $W_2$, $W_I$ AND $\phi_I$ the angular width of the overlap zone,

$$\phi_I = \pi - \phi_{\epsilon_1} - \phi_{\epsilon_2} ,$$

the apparent angle shift of each target may be calculated (it is the same for each target). All 6 cycles of target modulation are not

equally important (4). In fact, the $\pi$ radians of modulation must be weighted by the sin function from 0 to $\pi$. Figure 9A shows a typical $\pi$ radians of modulation, including a reduction for interference. Figure 9B shows the tracking effectiveness weighting and Fig. 9C the resultant of Fig. 9A and Fig. 9B. The center of energy in Fig. 9C is the effective target direction in the tracking system whereas in a non-interfering situation it would be the middle of the modulation, $\pi/2$. The formula for the shift in effective target tracking center, $\Delta\phi$, is:

$$\Delta\phi = \frac{\sin\phi_I - \frac{\pi}{2}(1 - \cos\phi_I) - \phi_I\left(1 - \frac{W_I}{W_1 + W_2}\right)\cos\phi_I}{I_R}, \quad 6)$$

where $I_R$, the effective energy reduction factor for both targets, is given by

$$I_R = \left| 1 + \cos\phi_I + \frac{W_I}{W_1 + W_2}(1 - \cos\phi_I) \right| \quad 7)$$

Finally, the effective target angle, $\phi_{\Delta_i}$, is:

$$\phi_{\Delta_1} = \phi_{\epsilon_1} + \Delta\phi \frac{\phi_{\epsilon_i} - \phi_{\epsilon_j}}{|\phi_{\epsilon_1} - \phi_{\epsilon_j}|}$$

It should be noted that the interference of two targets tends to increase the angle between the effective target tracking vectors. The solid vectors in Fig. 10 represent the effective tracking vector for each target in the absence of the other target. The dashed and primed vectors represent what happens when mutual interference is taken into consideration. In general there is a shift in resultant direction as well as a reduction in tracking rate (represented by the length of the vectors). Tracking rate calculations are given next. Using the interference reduction ratio, the effective tracking energy for each target is:

$$S_i E_i F_i I_R \quad 9)$$

The resultant effective seeker tracking in azimuth and elevation is obtained by:

$$S_a = I_R (S_1 E_1 F_1 \sin\phi_{\Delta_1} + S_2 E_2 F_2 \sin\phi_{\Delta_2}) \quad 10)$$

and

$$S_e = I_R (S_1 E_1 F_1 \cos\phi_{\Delta_1} + S_2 E_2 F_2 \cos\phi_{\Delta_2}) \quad 11)$$

Thus, the resultant tracking direction, $\phi_R$, and the resultant tracking rate, $K_p$, are:

$$\phi_R = \arctan \frac{S_a}{S_e} \qquad 12)$$

$$K_p = \frac{\sqrt{S_a^2 + S_e^2}}{I_R (S_1E_1F_1 + S_2E_2F_2) + N} \; K_{p_{max}} \; (I_R(S_1E_1F_1 + S_2E_2F_2) + N) \qquad 13)$$

where $K_{p_{max}}$ (X) is defined in (1).

(U) Many simplifications have been made in developing this digital simulation of two-target ATOLL tracking. While it is possible that there will be substantial errors at given instants of time or certain geometries, the average error should be low. Further work is being done on this problem and an improved model with N targets has been developed.

D. Fuze - Warhead Model

1. Fuze

(S) The ATOLL has a passive infrared fuze. It is a fixed, forward cone fuze at 76° from the missile axis with a fixed forward cone guard channel at 45° from the missile axis. This guard channel prevents the missile from fuzing on distant objects by requiring the guard channel pulse to occur no more than 25 ms before a fuzing channel pulse. The simulation calculates the times at which the flare and the tailpipe produce guard and fuze channel pulses, and from these times, determines when the warhead will explode. It is assumed that if the flare or tailpipe is close enough to satisfy the 25 millisecond criterion, it has enough energy to trigger the fuze.

(C) The following technique was used to determine accurate fuzing times. As the simulation proceeds along the missile trajectory, it tests the position of the flare and the tailpipe with respect to the position of the missile. When either the flare or the tailpipe passes through the fuze cone, the simulation selects either the time corresponding to the present position or to the last calculated position, whichever is closer in time to the instant at which the flare or tailpipe entered the fuze cone. At that point, the orientation of the missile body, the missile velocity and the target velocity are assumed constant (for fuzing time calculations only). The time until fuzing, $t_f$, is given by the following vector equation.

$$(\vec{V_T} - \vec{V_M})\Delta t_f \cdot \vec{B} + \vec{R}\cdot\vec{B} = \left| (\vec{V_t} - \vec{V_M})\Delta t_f + \vec{R} \right| \cos\theta$$

where $\vec{V}_T$ is the target velocity, $\vec{V}_M$ is the missile velocity, $\vec{B}$ is the missile body axis, $\vec{R}$ is the missile-to-target range vector and $\theta$ is the cone angle. This equation is quadratic in $\Delta t_f$, but the root with the smallest absolute value should be selected.

2. Warhead Blast

(S) No conventional lethality study is done here, but two criteria of flare success are used. If the warhead fragments have expanded more than 25 feet to reach the velocity vector of the target, or if they do not intersect the target path between the tail and the nose (i.e., pass behind or ahead) of the target, the flare is considered a success.

(S) The warhead ignites 5 ms after fuzing. This delay is added to the time of fuzing. From this point the warhead fragments expand in a ring at 6,050 ft/sec between the $80^\circ$ and $88^\circ$ forward cones with respect to the missile X-axis. This rate of expansion is assumed constant until the ring intersects the target flight path. The place the ring intersects the target X-axis is then used to determine whether the target was hit. The expansion distance of the fragments is the distance from the fragment ring to the current missile position when the ring intersects the path of the target. The expansion distance is used to estimate warhead lethality. The detonation of the warhead by a flare ejected shortly before missile impact is a major factor in flare effectiveness.

## III. Flare Effectiveness

### A. General

(U) This effectiveness study is exploratory in nature rather than definitive. Only a few situations are examined, some exhaustively, most superficially. Also, although the assumed flare characteristics were intended to represent the MK 46 flare, more recent measurements indicate that the MK 46 has considerably more IR energy output than used in this model. This study points out some of the problems of utilizing a flare against the ATOLL.

(U) This study uses individual simulated missile flights for data. The results of these flights are summarized in the "data plots" of Figs. 11-44. Each data plot is for a given altitude, missile launch speed, target speed, missile launch range, and target maneuver. Each plot is a polar plot in a horizontal plane through the target. The angle coordinate is the missile aspect angle at launch and the radial coordinate is missile-to-target range at the time a flare is ejected

or the time before missile launch that the flare is ejected. The summary plots in Figs. 45-56 are based on the data plots. The format of the summary plots is similar to the data plots except the flare ejection time (or range) data is summarized in blocks, and the radial coordinate is missile launch range.

B. Predetonation Effect

(S) The fuze in the ATOLL can be actuated by flares causing the warhead to detonate prematurely, thus significantly reducing lethality, even though parts of the missile may still strike its target. The condition for premature detonation is that the missile pass close to the flare. This can happen in two ways. First, if the flare is ejected while the missile is several thousand feet away, the missile may track the flare instead of the target and come close to the flare. This decoy action will be discussed later. Secondly, if the flare is ejected so that its trajectory is through the rather limited zone where the ATOLL must make its terminal approach, the missile and flare will come close together. While current flare dispensers are not designed to do this, they do have significant capability in this area. There does not appear to be a problem in making a flare which radiates enough energy to activate a fuze by the time the flare falls behind the target.

(S) To find the potential effectiveness of predetonation of the warhead, the question is asked, "How close can we allow the ATOLL to come and still eject a flare which will detonate the warhead behind our aircraft?" The answer is "as close as 100 feet" for some cases. For example, Fig. 46 shows that when a missile is launched at a range of 5000 ft and at an aspect angle of 170°, a flare (from the left hand ejector) ejected when the missile has closed to 100 ft will explode the warhead behind the aircraft. The same figure shows that if the launch range is reduced to 3000 ft, the flare should be released when the missile is no closer than 200 ft. This is not surprising, since the minimum missile range at which a flare is effective is simply that range which allows the flare sufficient time to get behind the target and for the missile to fuze and explode before it gets to the target. This distance is a function of how fast the missile is closing on the target - the faster the missile, the longer the distance must be. Since the shortest launch ranges result in the fastest missiles at target intercept, they also result in the longest ranges for flare predetonation effectiveness. Figure 54 illustrates this effect very well.

(S) This phenomenon leads to the following argument: Since the maximum missile ranges for flare ejection occur at the minimum missile launch ranges, and since the greatest minimum flare ejection range under the conditions in this study is 500 ft (Fig. 53), then if the flare is ejected when the missile is at a range of 500 ft, the missile will always be defeated. Unfortunately, this simple

solution does not work. First, Fig. 55 shows that the minimum missile range for successful flare ejection has increased for increased missile launch range to 1100 ft (and higher in other cases). Here the flare is far enough from the missile trajectory that the lower missile speed produces a fuze pulse which occurs too long after the guard pulse to cause fuzing. (Most of these situations occur when the target is maneuvering.) Secondly, in the case where ATOLL is launched 20° off the tail and at 600 ft launch range as shown on Fig. 51, there is only an instant at a range 250 ft when the flare will cause predetonation. In this case, 500 ft is too long a range for flare ejection. No solution to the problem of when to eject the flare for 100% predetonation effectiveness has been discovered.

(S) The flare ejection control problem does not seem to have any simple answer. Even if the 500 ft ejection range worked perfectly, or if any range was considered to be adequately effective, it seems unlikely that a pilot could see the missile then or accurately gauge its range if he could. Thus some form of radar sensor would be required to detect the missile and measure its range. Such a sensor could initiate the deployment of chaff as well as flares to counter active radar or optically fuzed missiles as well as the ATOLL.

(C) The detonation of the ATOLL warhead does not immediately cause the missile to disintegrate. Rather the seeker/control section and the motor/tail section often continue intact along the missile trajectory. Thus, although no warhead fragment may strike the target when the flare predetonates the warhead, one or both of these missile sections may. The probability of significant damage from these pieces seems low and is ignored in this study.

C. Decoy Effect

(S) The ordinary application of an infrared flare is to decoy the missile from the target to the flare. This study shows that this can be done effectively over a wide range of conditions. In this part of the report, in addition to discussing how well the flare performs as a decoy, the requirements for accuracy in the time of flare ejection and the requirements on the length of flare burn time are discussed.

(C) The required accuracy for the time of flare ejection is determined by the length of the time interval during which a flare ejection would effectively counter the ATOLL. This interval of success may start before missile launch. If a series of flares were ejected at this interval, ATOLL would be ineffective. This is generally impracticable, since the aircraft cannot carry the required large number of flares. For this reason, the study did not consider multiple flares. Therefore the time intervals of success which are determined define the magnitude of the problem, but not a solution.

(S) One of the most significant facts about the effective decoy time intervals is that they all include the missile launch time. Although the intervals may vary from 1.2 to 10.4 s, depending upon the tactical conditions, a flare ejected precisely at missile launch always did decoy the ATOLL. However, in 2 of the 39 intervals which were calculated, if a flare were ejected 0.1 second after missile launch, it would fail. These cases are shown in Fig. 50, 6000 feet launch range, $10^{o}$ off the tail and Fig. 52, 3000 feet launch range, $10^{o}$ off the tail. Thus a missile launch detector should prove very effective if used to automatically eject a flare. If a missile launch detector could eject a flare within 2 seconds after the ATOLL motor is ignited, the flare would be successful in 87% of the cases on Figs. 49-52.

(S) The ejection intervals of success vary substantially, but the principal variation is due to missile launch range. As would be expected, the longer the missile flight time, the longer the time available for successful flare ejection. Generally the intervals are about 3 seconds for minimum missile launch ranges, and about 9 seconds for maximum launch ranges. While these intervals are occasionally much shorter than the missile launch range would indicate, a radar sensor that automatically ejected flares at intervals dependent upon the range to the attacker would be effective if the pilot (or the radar) can stop the flare ejections when the attacker is not in ATOLL launch zone.

(S) The required burn time for a flare is important, since the size of a flare is fixed by available dispensers and burn time is traded off with infrared output. Current flares have adequate infrared output in the ATOLL band in relation to the infrared output of aircraft engines at military power. Two criteria for required flare burn time are calculated. One of these criteria is quite conservative and requires the flare to burn until the missile passes it, while the other criterion only requires that the target be out of the missile's field of view. The data shown in Figs. 49-52 with respect to these two criteria are the longest times of all the successful flares. Thus a shorter burn time might prove almost as effective. In only 2 of the 39 data points did the requirement that the flare burn until the missile passed the flare exceed the 6.5 s burn of the simulated flare. The less stringent requirement that the flare burn until the target is out of the field of view produces a maximum burn time of 5.7 for all 39 cases. Other less stringent criteria, which might allow a reduction of burn time, seem reasonable and worthy of further investigation.

D. Holes

(S) There are regions along the trajectory of the missile where a flare is ineffective. These regions interlace with regions where the flare is effective. These "holes" in flare performance are not random,

but may be too complex to calculate in an airborne environment. They greatly complicate the flare ejection control problem. Further study is required to determine whether these holes can be eliminated by flare or dispenser modification, predicted by an airborne countermeasures control device, or simply ignored and lumped with the random effects.

E. Ejection Direction

(S) The F-4B aircraft has 2 ALE-29 flare ejectors which eject flares about $37^{\circ}$ above the horizontal plane of the aircraft on either side of the fuselage. A comparison of the effectiveness of these two dispensers, shown in Fig. 50 for a non-maneuvering F-4B, shows a large (3 to 1) loss in effectiveness when the flare is ejected on the opposite side from that which the ATOLL is approaching. No trend is apparent in the maneuvering F-4B data shown in Fig. 52 where the flares are ejected either up or inside the turn due to the $70^{\circ}$ bank angle required for a 3-g turn. Either direction appears about as effective as ejection toward the missile in the non-maneuvering case.

(S) The data in Figs. 47 and 51 for the F-8 aircraft, where the flare is ejected downward from the aircraft, indicate no significant differences in flare effectiveness due to maneuver. Neither is there a significant difference between the F-4B and the F-8 in overall flare effectiveness.

IV. Conclusions

(1)(S) Currently available infrared flares (MK 46) provide the F-4B and F-8 aircraft with substantial protection against the ATOLL when they are operating without afterburner.

(2)(S) An automatic missile launch detector coupled to a flare ejection control is needed to fully utilize the capability of the flare.

(3)(S) Flare effectiveness is complex and difficult to predict with simple models.

(4)(S) The direction of flare ejection is a significant factor in flare effectiveness.

## V. Recommendations

(1)(S) Since infrared flares are an effective countermeasure to ATOLL, they should be made available to operating squadrons.

(2)(S) The potential of infrared flares as countermeasure to ATOLL should be further investigated.

(3)(U) The requirements for a rear-looking sensor for aircraft and missile detection and for automatic countermeasures control should be investigated.

(4)(S) Alternative ATOLL countermeasures should be investigated, especially those with potential effectiveness against a minimum range missile launch.

## References

(Titles Unclassified)

(1) H. Toothman, C. Loughmiller, and R. Lister, "The Effect of F-4B Maneuvers on ATOLL (AA-2) Performance," NRL Memorandum Report 1989, Secret-Noforn, Feb. 1969.

(2) H. Toothman and C. Loughmiller, "The Effect of F-8 Maneuvers on ATOLL (AA-2) Performance," NRL Memorandum Report 2170, Secret-Noforn.

(3) E. Raisen, "Effects of Wind and Altitude on the Behavior of Infrared Decoy Flares," Proceedings of the Sixth Symposium on Infrared Countermeasures, Volume 2, Secret-Noforn, April 1967.

(4) W. C. Fitzgerald and R. E. Lawrence, "Sidewinder Optical Systems," NAVWEPS Report 8524, Secret, March 1965.

Acknowledgements

(Unclassified)

The authors acknowledge the following people for their help in getting the work done. The authors assume full responsibility for the accuracy of this report.

Westinghouse Aerospace Division
Arthur Harvey for the realization of the model in computer language
Howard Noble for the reduction of the data
Elmen Quesinberry for the work in modeling the flare and seeker

NWCCL
George Handler for supplying flare information

NRL
Jacqueline Imes and Richard Lister for preparing the figures

## Distribution List

(Unclassified)

| | | |
|---|---|---|
| CNO | OP-506G | 1 |
| | OP-724D | 1 |
| | OP-72402 | 1 |
| | OP-07T | 1 |
| NAVAIRSYSCOM | AIR-53365C | 5 |
| | AIR-5363 | 1 |
| | AIR-360C | 1 |
| | AIR-5333CE | 1 |
| | AIR-53221 | 1 |
| | AIR-5363IF | 1 |
| CNM | PM-73 | 1 |
| | 0323A | 1 |
| NWC-CL | G. Handler | 1 |
| | K. Powers | 1 |
| | W. Younkin | 1 |
| NMC | 5230 | 1 |
| | 5311 | 1 |
| NRL | 5117 | 1 |
| NAD, Crane | 1000 | 1 |
| NOL-WO | E. Dayhoff | 1 |
| | R. Hebbert | 1 |
| Airtronics/SWL | G. Morin | 1 |
| Westinghouse Aerospace Division<br>Friendship Airport<br>Baltimore, Md. | E. C. Quesinberry | 1 |
| Defense Documentation Center<br>Attn TIPDR | | 2 |

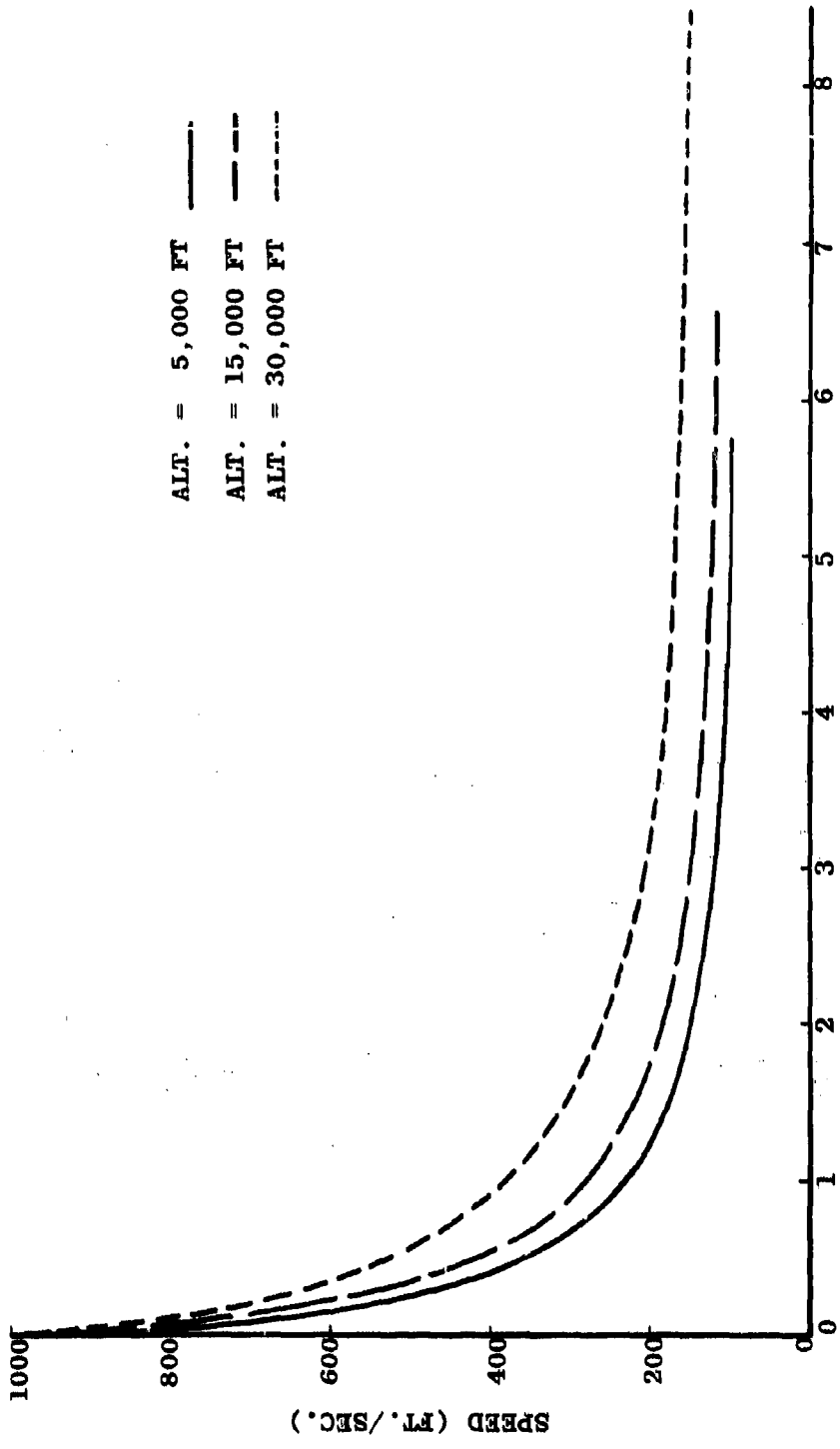


FIG. 1 - SLOWDOWN OF SIMULATED FLARE (C)

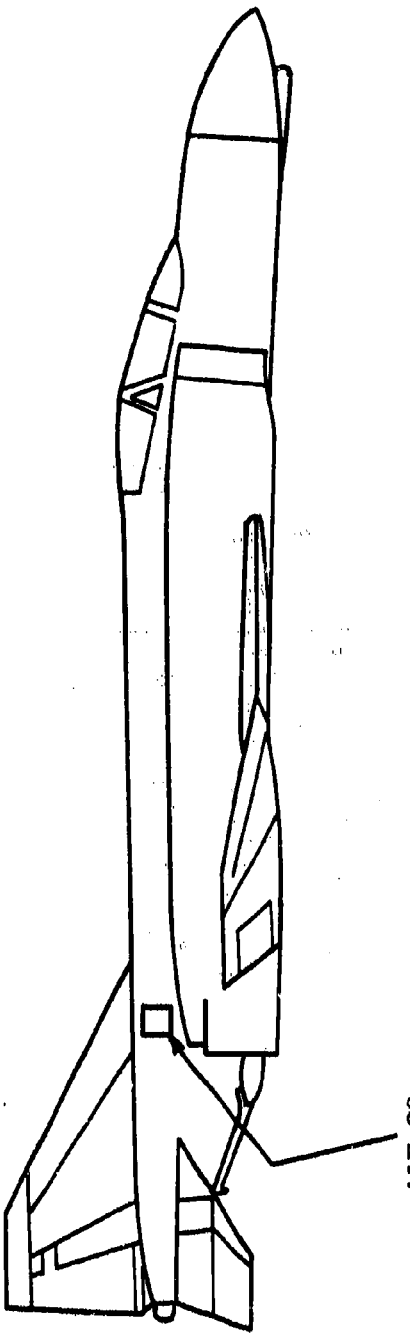


FIG. 2 - F-4 FLARE DISPENSER LOCATION (C)

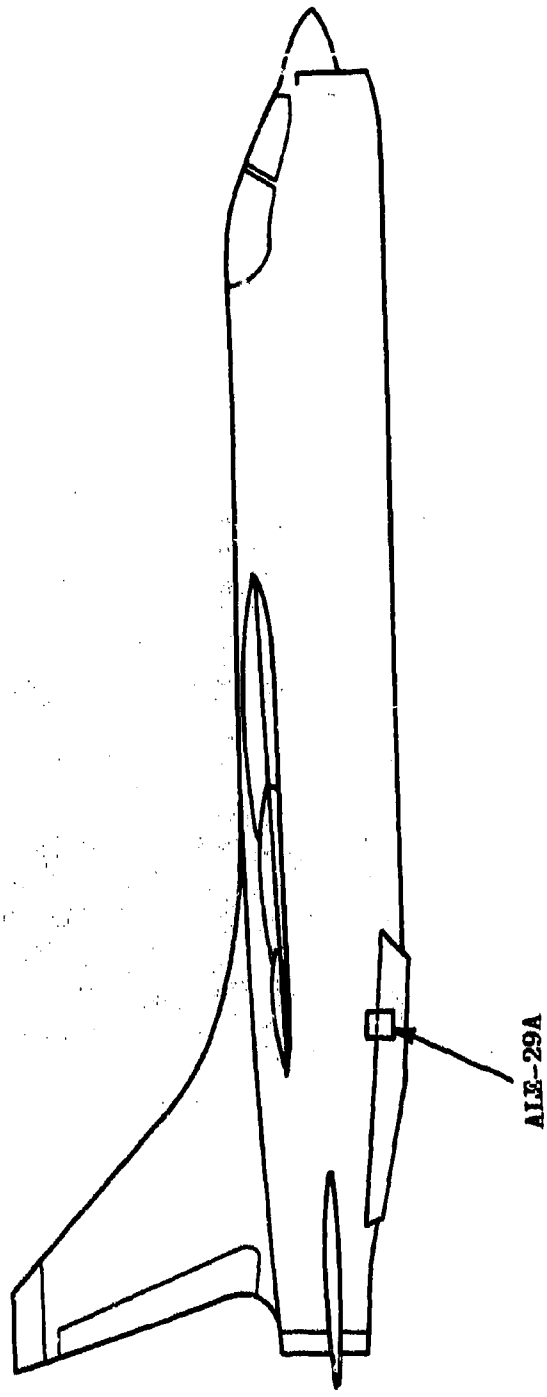


FIG. 3 - F-8 FLARE DISPENSER LOCATION (C)

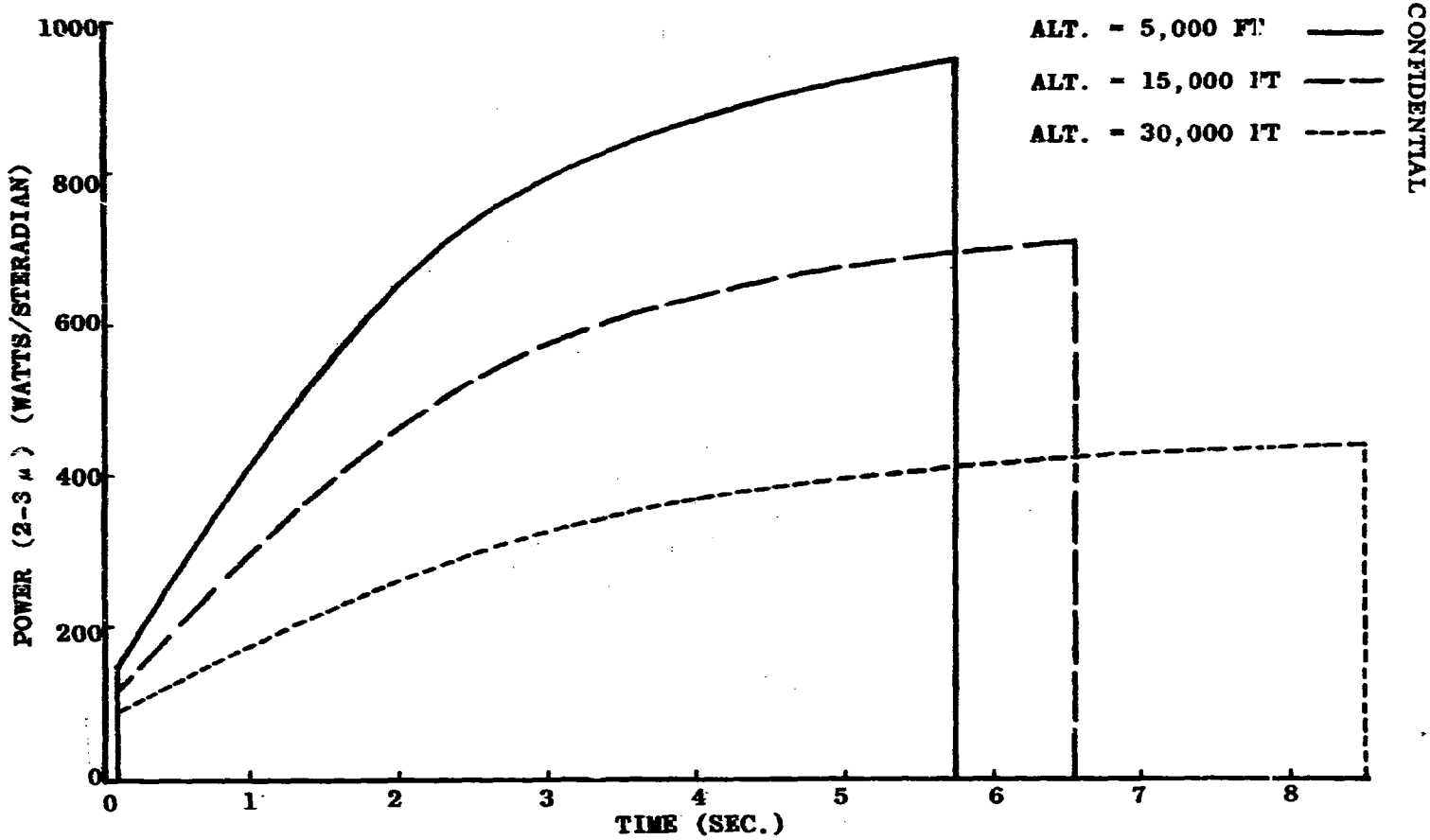


FIG. 4 - SIMULATED FLARE RADIANT INTENSITY (C)

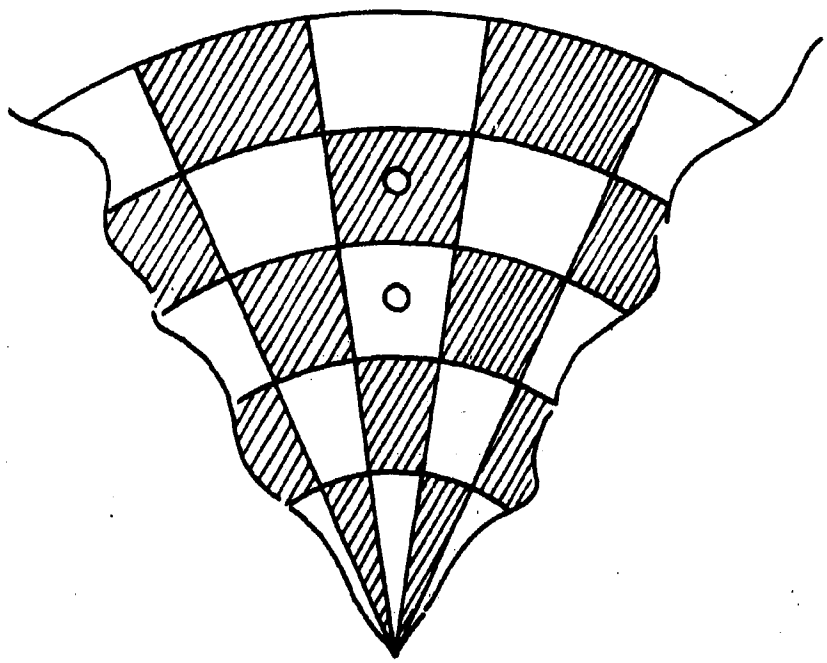

FIG. 5 - TWO TARGETS WITH NO TRACKING (U)

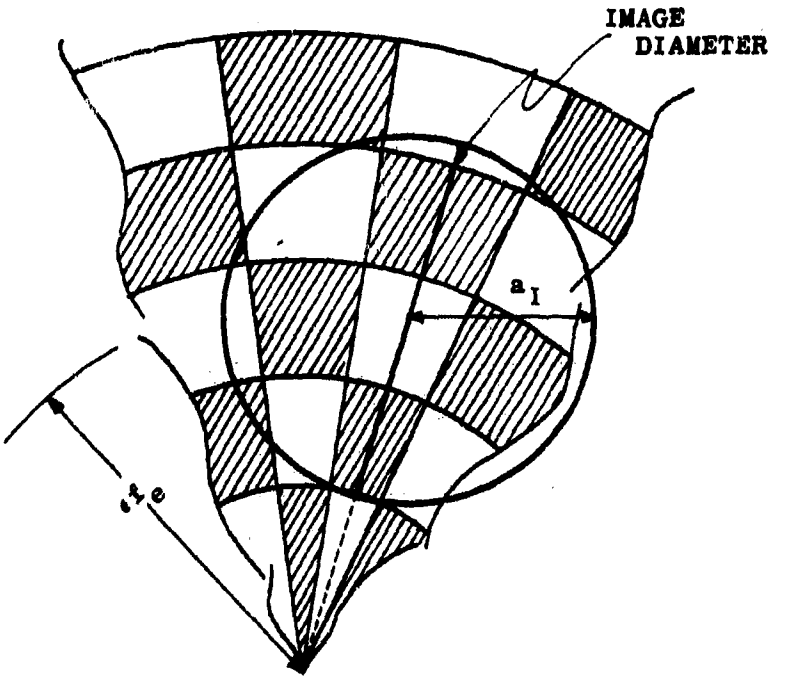


FIG. 6 - RADIAL EFFICIENCY DIAGRAM (U)

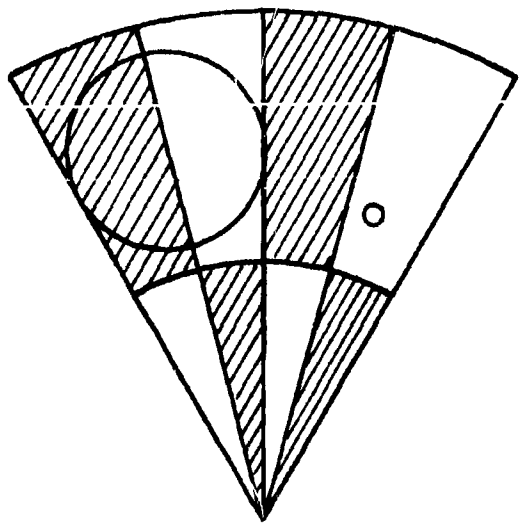

A. RETICLE AND TARGET PICTURE

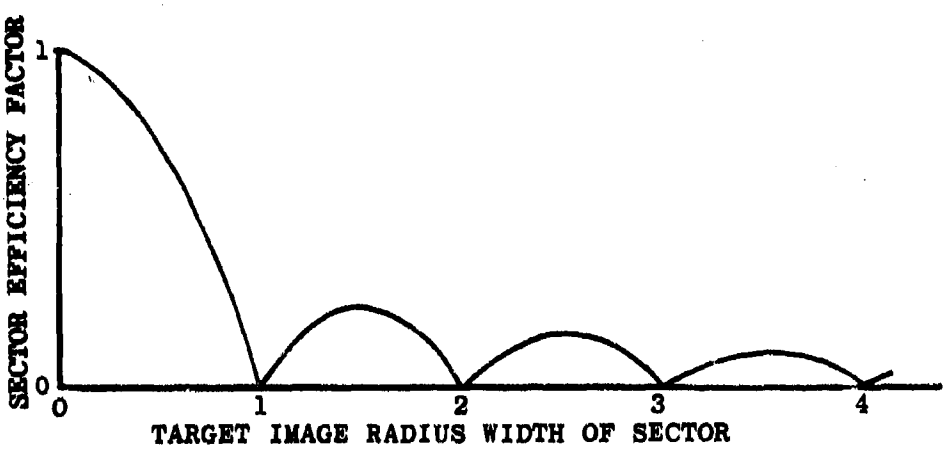


B. SECTOR EFFICIENCY FACTOR VS. IMAGE SIZE

FIG. 7 - RETICLE MODULATION EFFICIENCY MODEL (U)

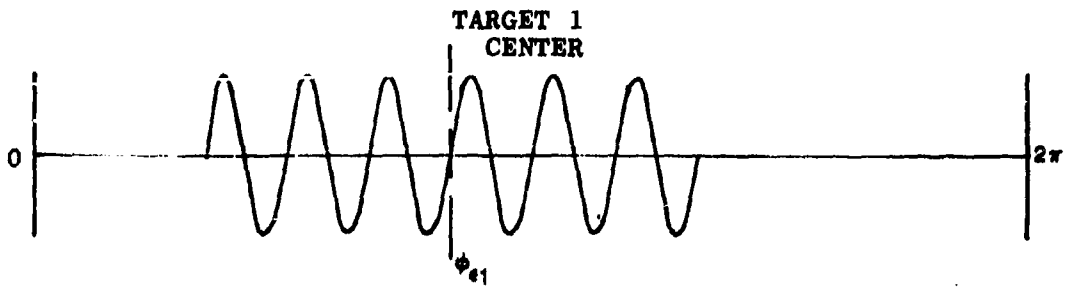


A. TARGET 1 SIGNAL

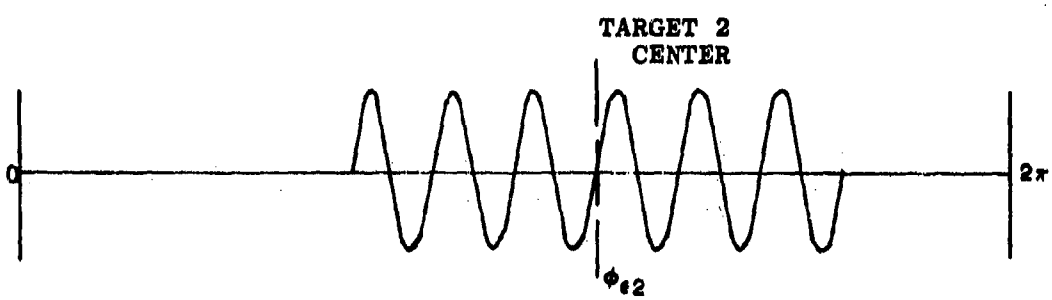


B. TARGET 2 SIGNAL

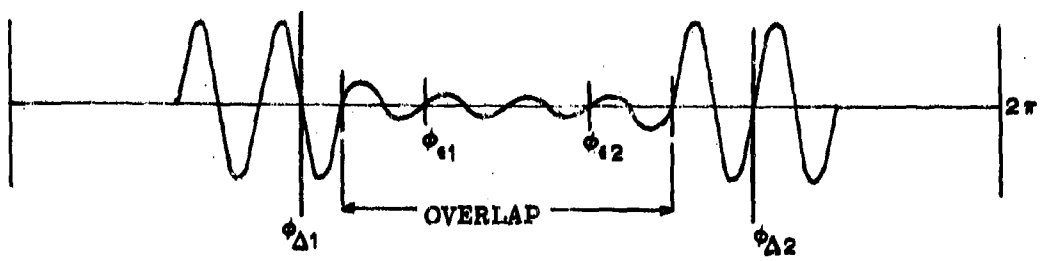


C. RESULTANT SIGNAL

FIG. 8 - TARGET INTERFERENCE IN THE PHOTOCELL (U)

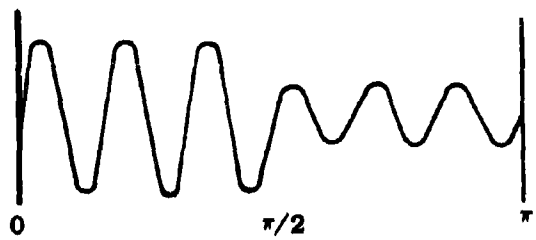


A. EFFECTIVE TARGET MODULATION

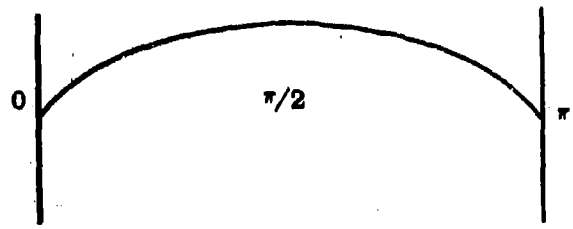


B. WEIGHTING FUNCTION FOR TRACKING EFFECTIVENESS

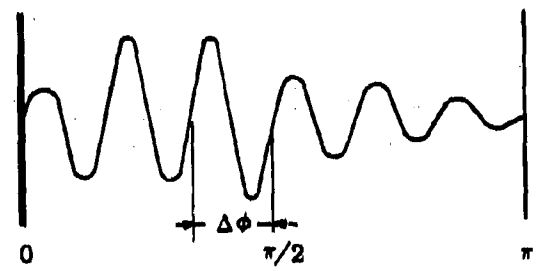


C. RESULTING SHIFT OF CENTER OF TRACKING, $\Delta\phi$

FIG. 9 - CENTER OF ENERGY SHIFT (U)

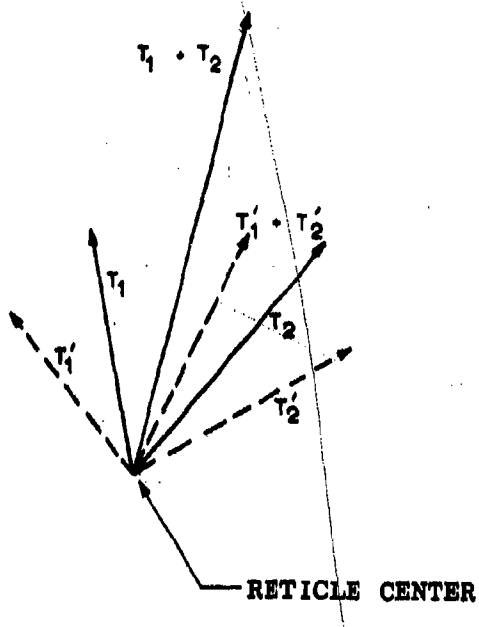


FIG. 10 - VECTORS REPRESENT TRACKING RATES (U)

× DECOY SUCCESS
△ PREDETONATION SUCCESS
○ FLARE FAILURE

F-8
ALTITUDE = 5,000 FT
LAUNCH RANGE = 3,000 FT
LAUNCH SPEED = M 0.9
TARGET SPEED = M 0.9
NO MANEUVER

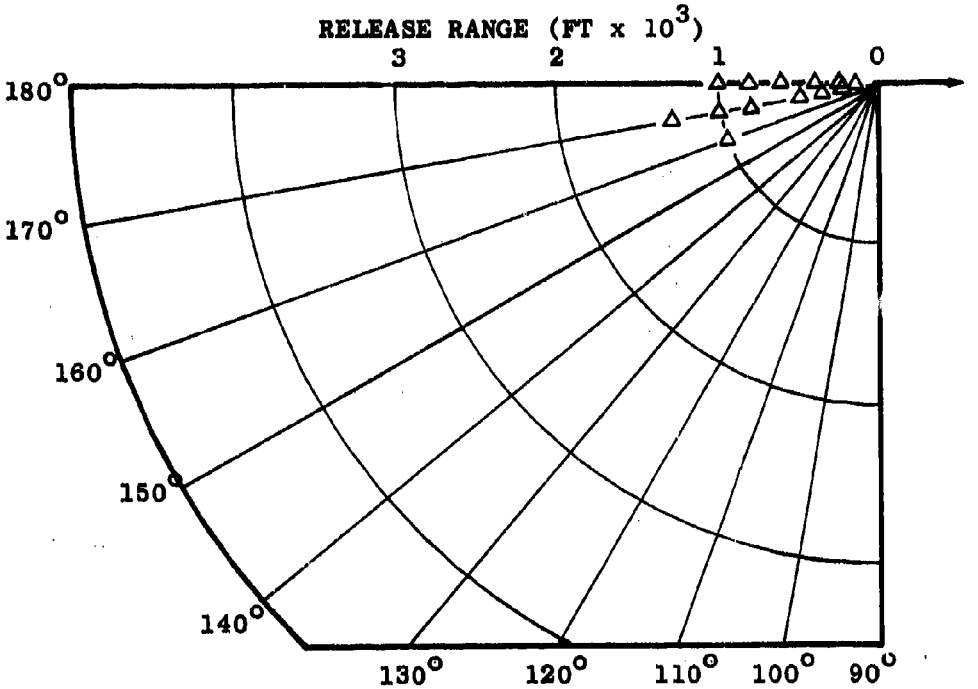


FIG. 11 - FLARE SUCCESS VERSUS FLARE EJECTION TIME (S)

× DECOY SUCCESS
△ PREDETONATION SUCCESS
○ FLARE FAILURE

F-8
ALTITUDE = 5,000 FT
LAUNCH RANGE = 5,000 FT
LAUNCH SPEED = M 0.9
TARGET SPEED = M 0.9
NO MANEUVER

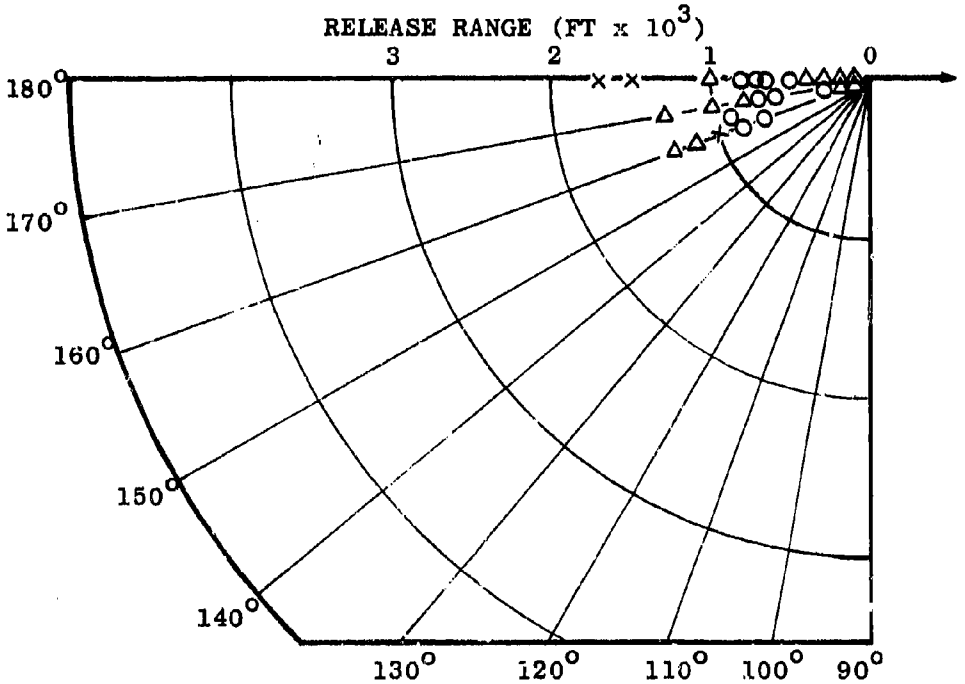


FIG. 12 - FLARE SUCCESS VERSUS FLARE EJECTION TIME (S)

× DECOY SUCCESS
△ PREDETONATION SUCCESS
○ FLARE FAILURE

F-8
ALTITUDE - 5,000 FT
LAUNCH RANGE - 3,000 FT
LAUNCH SPEED - M 0.9
TARGET SPEED - M 0.9
3g TURN

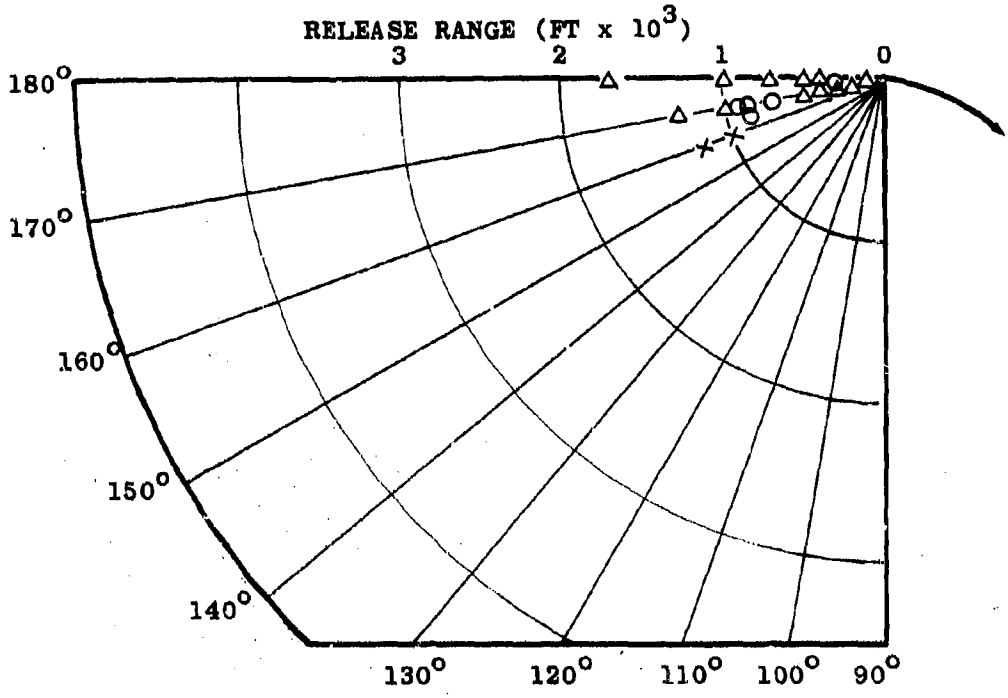


FIG. 13 - FLARE SUCCESS VERSUS FLARE EJECTION TIME (S)

× DECOY SUCCESS
△ PREDETONATION SUCCESS
○ FLARE FAILURE

F-8
ALTITUDE = 5,000 FT
LAUNCH RANGE = 5,000 FT
LAUNCH SPEED = M 0.9
TARGET SPEED = M 0.9
3g TURN

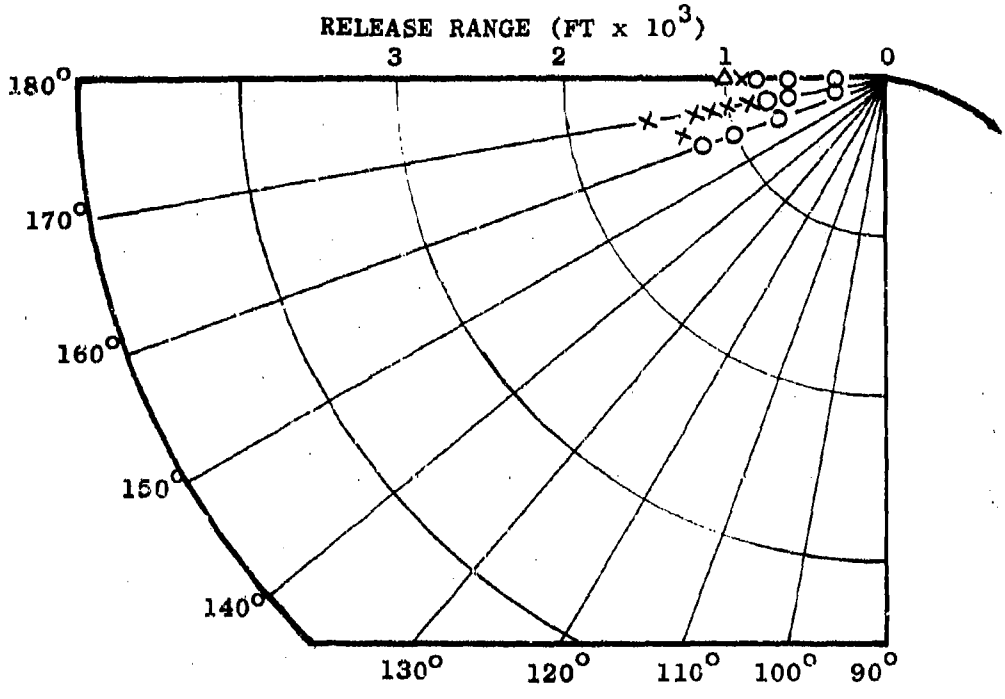


FIG. 14 - FLARE SUCCESS VERSUS FLARE EJECTION TIME (S)

× DECOY SUCCESS
△ PREDETONATION SUCCESS
○ FLARE FAILURE

F-8
ALTITUDE = 15,000 FT
LAUNCH RANGE = 3,000 FT
LAUNCH SPEED = M 1.2
TARGET SPEED = M 0.9
NO MANEUVER

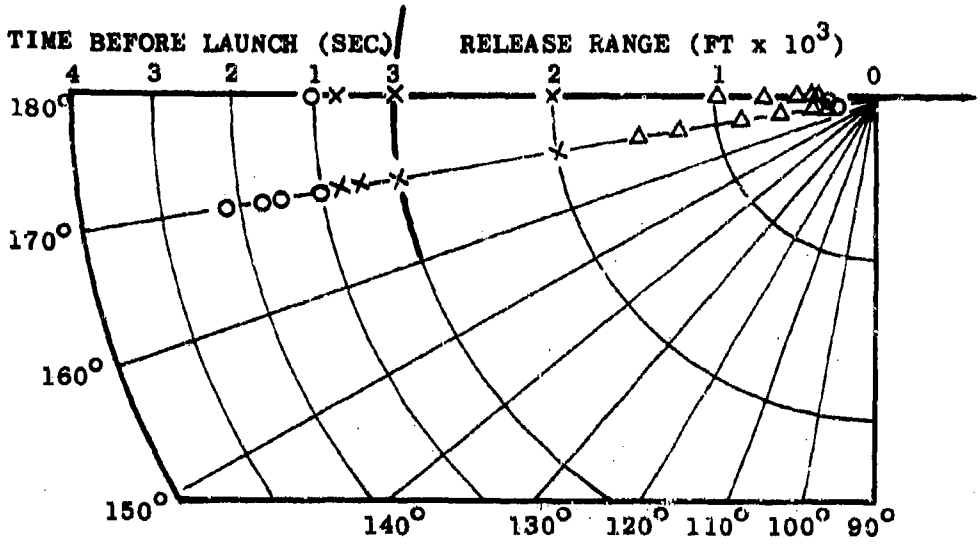


FIG. 15 - FLARE SUCCESS VERSUS FLARE EJECTION TIME (S)

× DECOY SUCCESS
△ PREDETONATION SUCCESS
○ FLARE FAILURE

-8
ALTITUDE = 15,000 FT
LAUNCH RANGE = 6,000 FT
LAUNCH SPEED = M 1.2
TARGET SPEED = M 0.9
NO MANEUVER

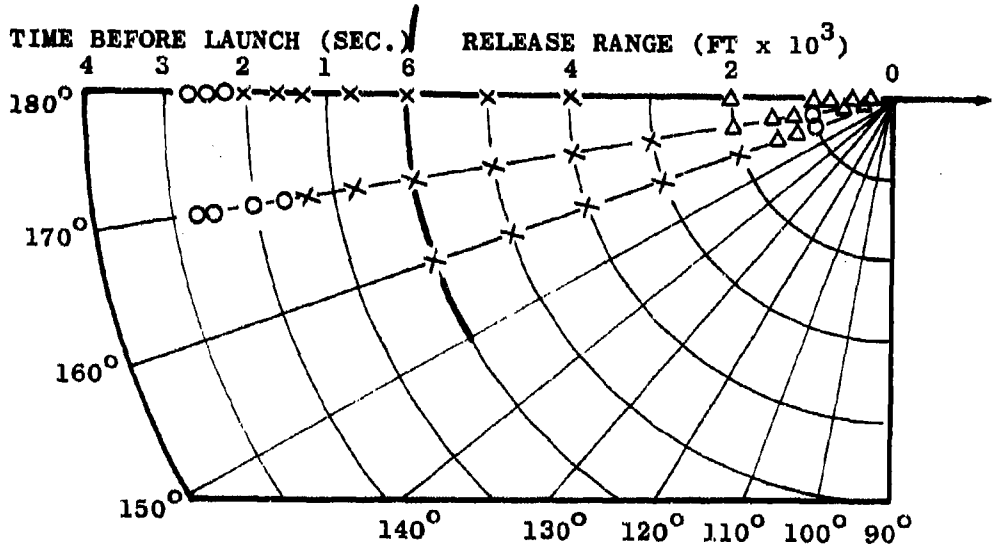


FIG. 16 - FLARE SUCCESS VERSUS FLARE EJECTION TIME (S)

× DECOY SUCCESS
△ PREDETONATION SUCCESS
○ FLARE FAILURE

F-8
ALTITUDE = 15,000 FT
LAUNCH RANGE = 7,000 FT
LAUNCH SPEED = M 1.2
TARGET SPEED = M 0.9
NO MANEUVER

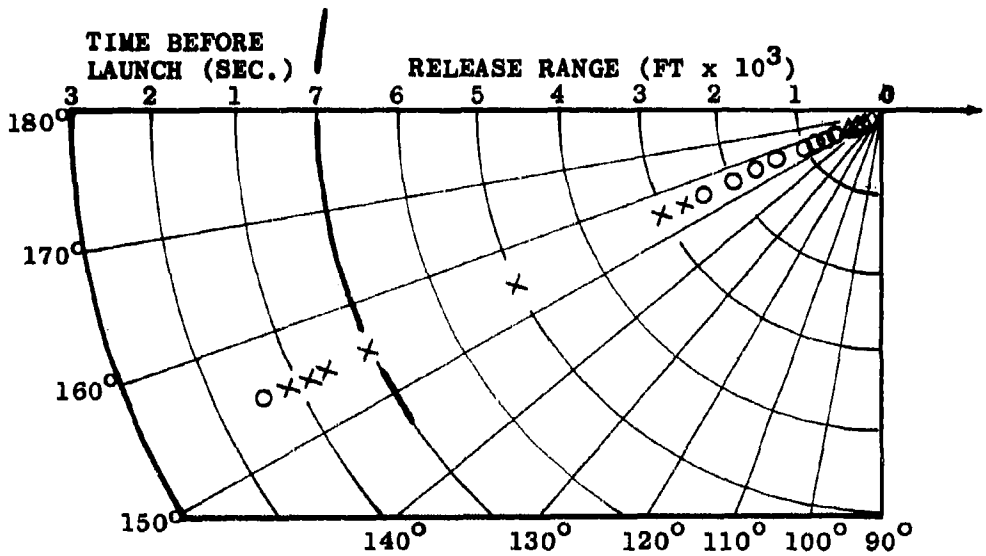


FIG. 17 - FLARE SUCCESS VERSUS FLARE EJECTION TIME (S)

× DECOY SUCCESS
△ PREDETONATION SUCCESS
○ FLARE FAILURE

F-8
ALTITUDE - 15,000 FT
LAUNCH RANGE - 8,000 FT
LAUNCH SPEED - M 1.2
TARGET SPEED - M 0.9
NO MANEUVER

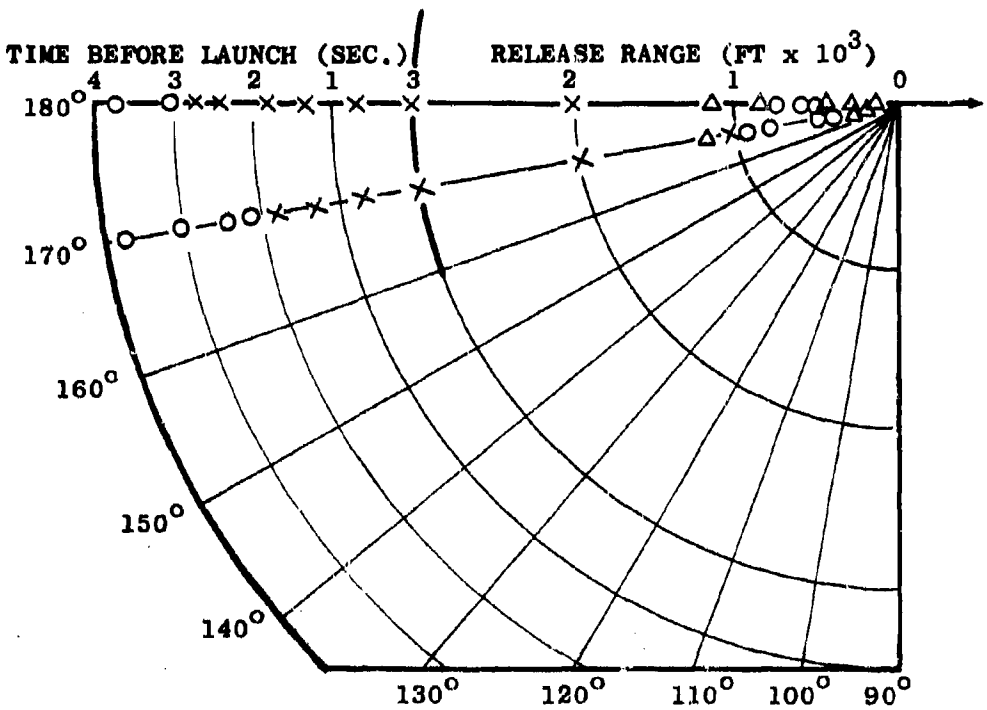


FIG. 18 - FLARE SUCCESS VERSUS FLARE EJECTION TIME (S)

× DECOY SUCCESS
△ PREDETONATION SUCCESS
○ FLARE FAILURE

F-8
ALTITUDE = 15,000 FT
LAUNCH RANGE = 3,000 FT
LAUNCH SPEED = M 1.2
TARGET SPEED = M 0.9
3g TURN

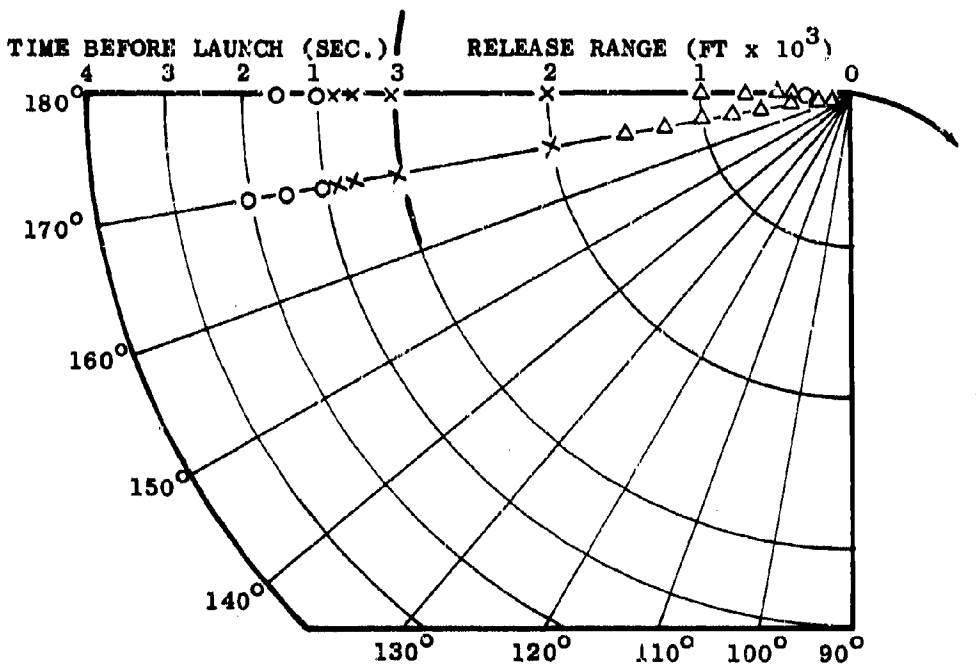


FIG. 19 - FLARE SUCCESS VERSUS FLARE EJECTION TIME (S)

× DECOY SUCCESS
△ PREDETONATION SUCCESS
○ FLARE FAILURE

F-8
ALTITUDE = 15,000 FT
LAUNCH RANGE = 6,000 FT
LAUNCH SPEED = M 1.2
TARGET SPEED = M 0.9
3g TURN

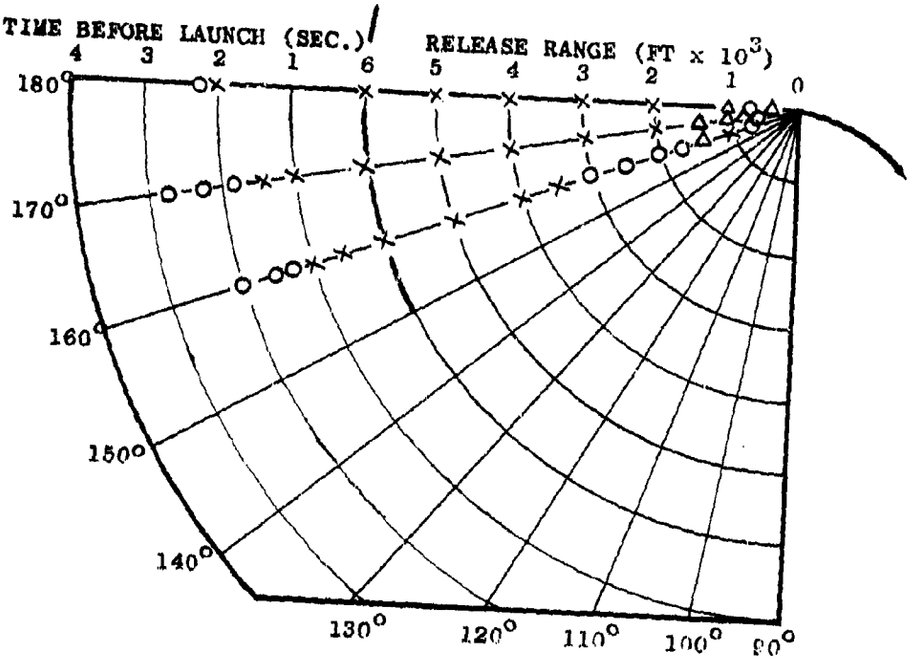


FIG. 20 - FLARE SUCCESS VERSUS FLARE EJECTION TIME (S)

× DECOY SUCCESS
△ PREDETONATION SUCCESS
○ FLARE FAILURE

F-8
ALTITUDE = 15,000 FT
LAUNCH RANGE = 8,000 FT
LAUNCH SPEED = M 1.2
TARGET SPEED = M 0.9
3g TURN

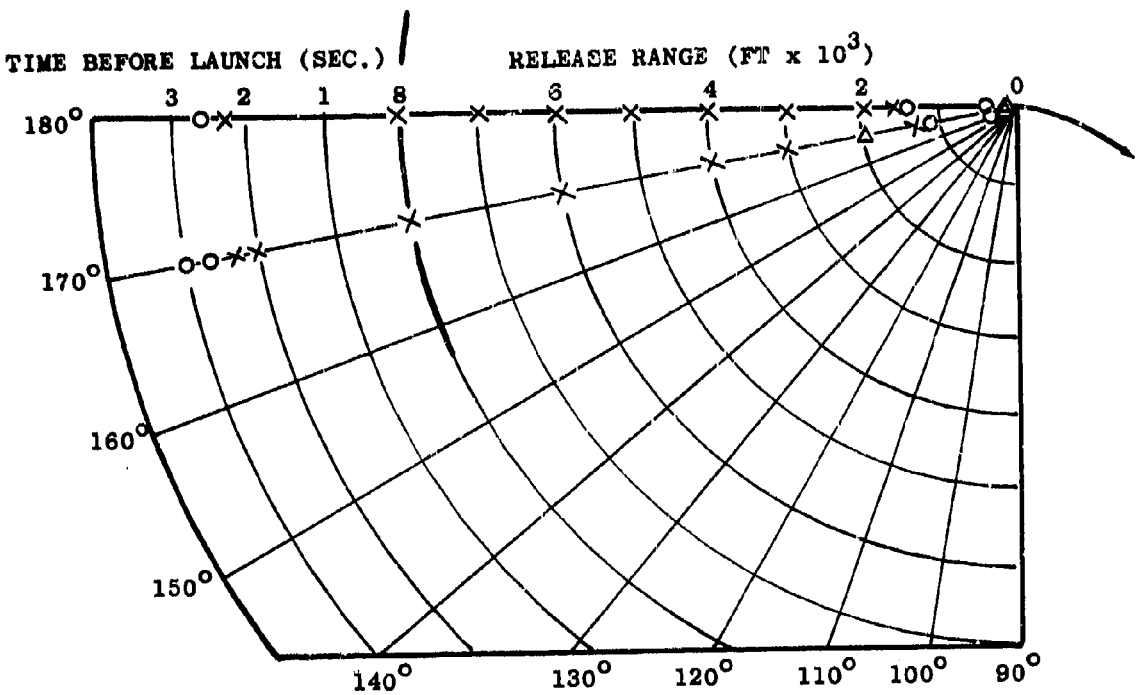


FIG. 21 - FLARE SUCCESS VERSUS FLARE EJECTION TIME (S)

× DECOY SUCCESS
△ PREDETONATION SUCCESS
○ FLARE FAILURE

F-8
ALTITUDE = 30,000 FT
LAUNCH RANGE = 4,000 FT
LAUNCH SPEED = M 1.2
TARGET SPEED = M 0.9
NO MANEUVER

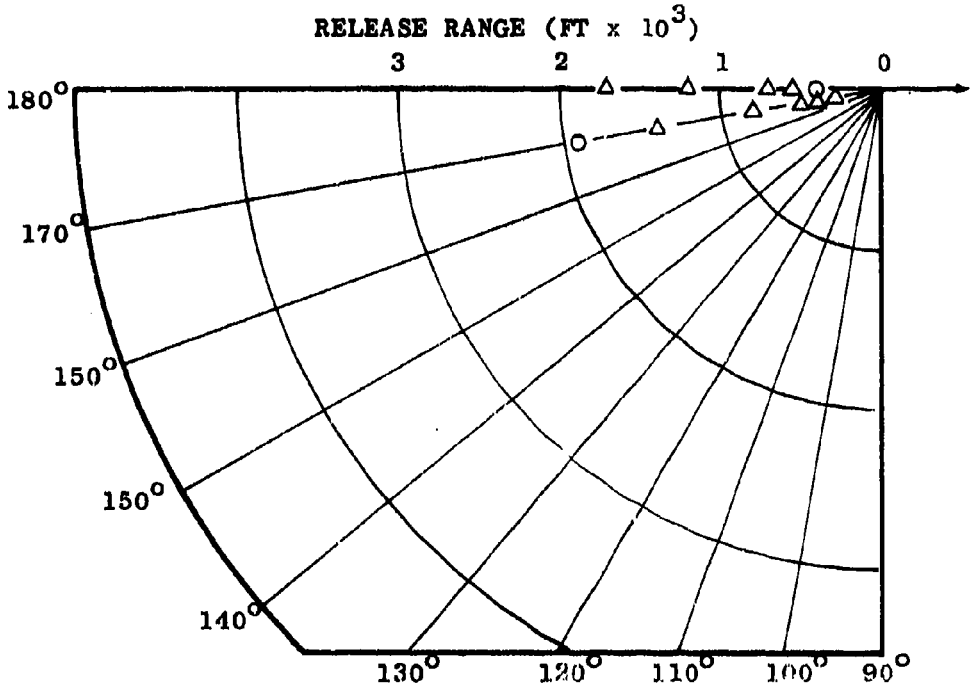


FIG. 22 - FLARE SUCCESS VERSUS FLARE EJECTION TIME (S)

× DECOY SUCCESS
△ PREDETONATION SUCCESS
○ FLARE FAILURE

F-8
ALTITUDE = 30,000 FT
LAUNCH RANGE = 8,000 FT
LAUNCH SPEED = M 1.2
TARGET SPEED = M 0.9
NO MANEUVER

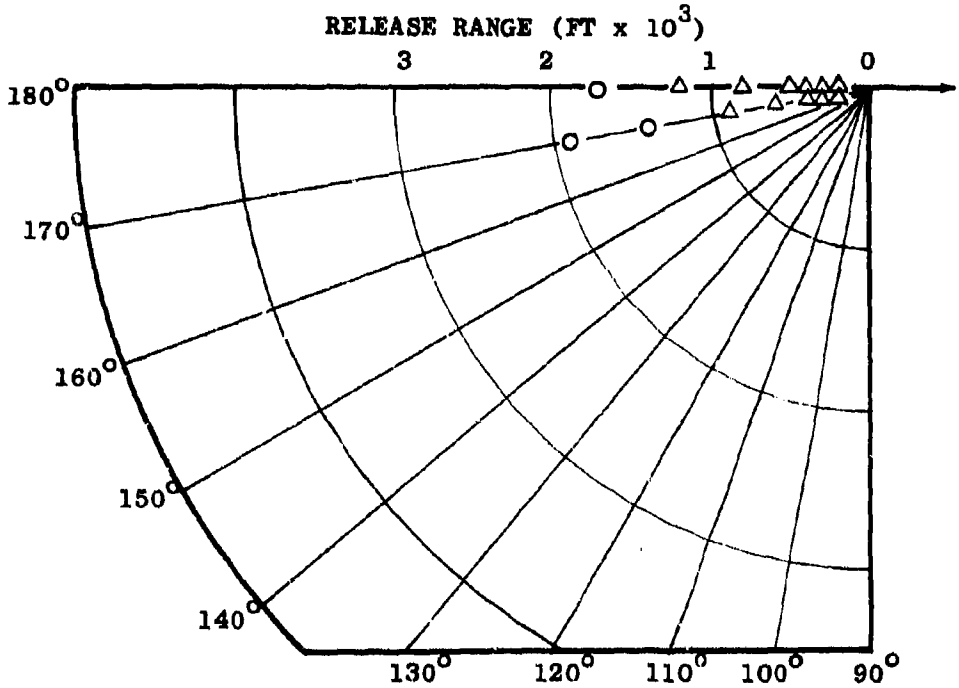


FIG. 23 - FLARE SUCCESS VERSUS FLARE EJECTION TIME (S)

× DECOY SUCCESS
△ PREDETONATION SUCCESS
○ FLARE FAILURE

F-8
ALTITUDE = 30,000 FT
LAUNCH RANGE = 12,000 FT
LAUNCH SPEED = M 1.2
TARGET SPEED = M 0.9
NO MANEUVER

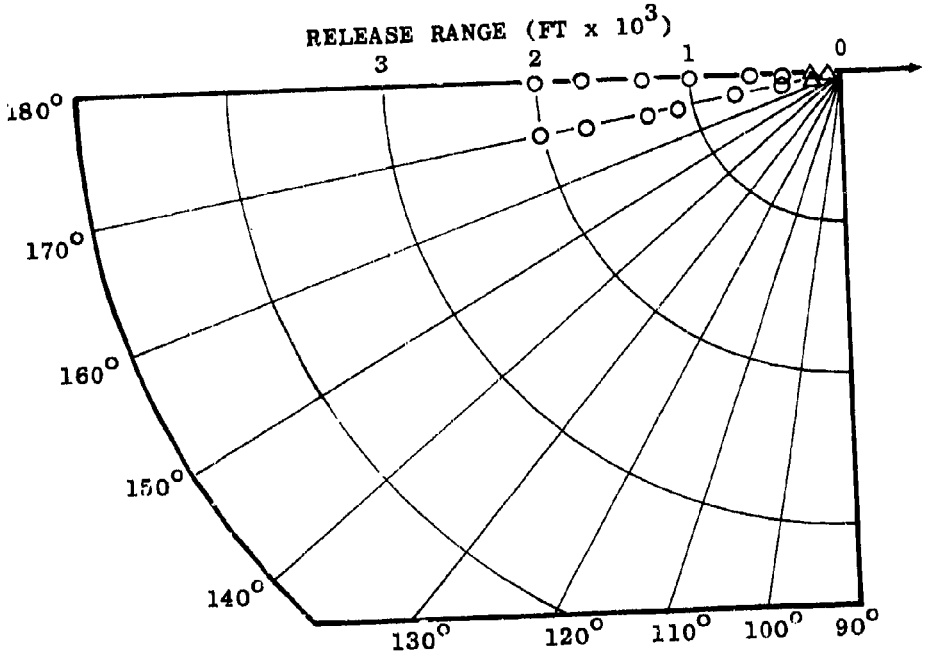


FIG. 24 - FLARE SUCCESS VERSUS FLARE EJECTION TIME (S)

× DECOY SUCCESS
△ PREDETONATION SUCCESS
○ FLARE FAILURE

F-8
ALTITUDE = 30,000 FT
LAUNCH RANGE = 4,000 FT
LAUNCH SPEED = M 1.2
TARGET SPEED = M 0.9
3g TURN

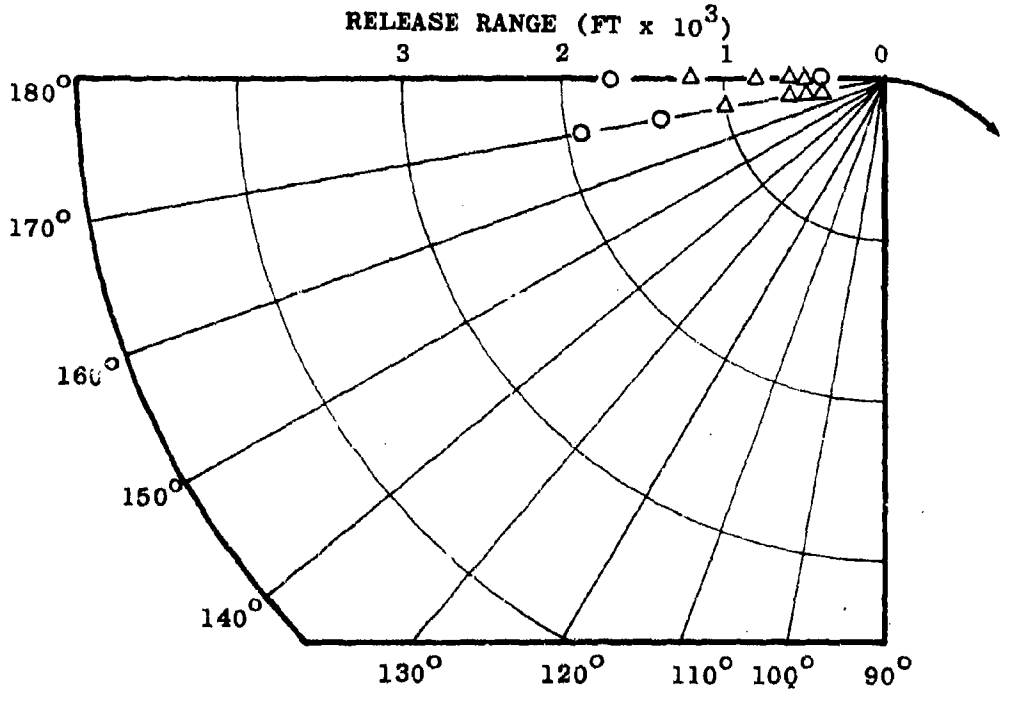


FIG. 25 - FLARE SUCCESS VERSUS FLARE EJECTION TIME (S)

× DECOY SUCCESS
△ PREDETONATION SUCCESS
○ FLARE FAILURE

F-8
ALTITUDE = 30,000 FT
LAUNCH RANGE = 8,000 FT
LAUNCH SPEED = M 1.2
TARGET SPEED = M 0.9
3g TURN

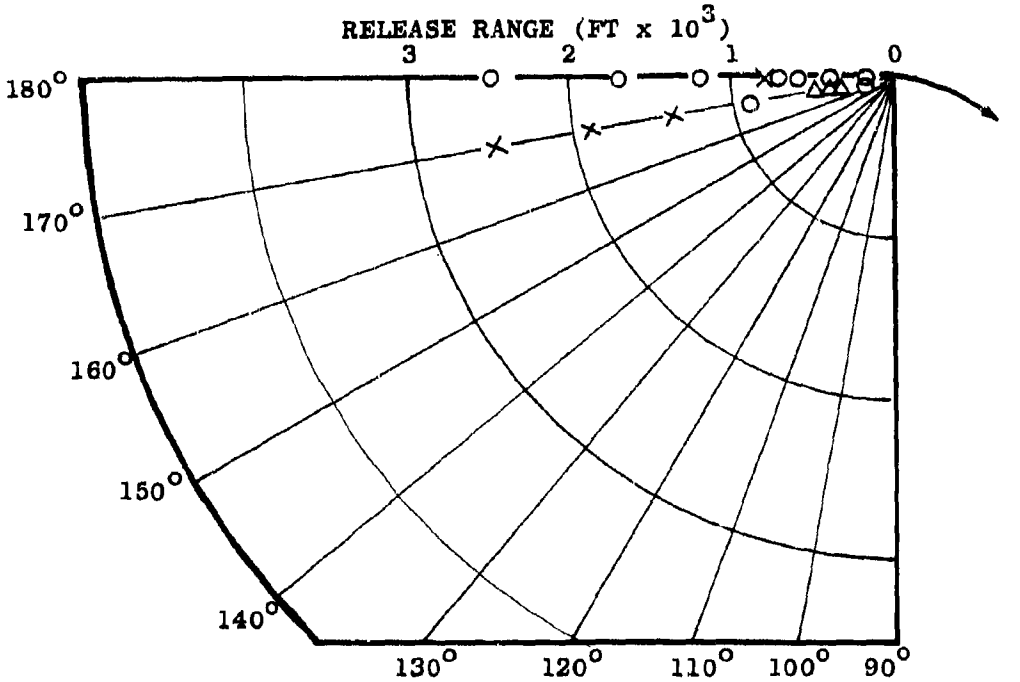


FIG. 26 - FLARE SUCCESS VERSUS FLARE EJECTION TIME (S)

× DECOY SUCCESS
△ PREDETONATION SUCCESS
○ FLARE FAILURE

F-8
ALTITUDE = 30,000 FT
LAUNCH RANGE = 12,000 FT
LAUNCH SPEED = M 1.2
TARGET SPEED = M 0.9
3g TURN

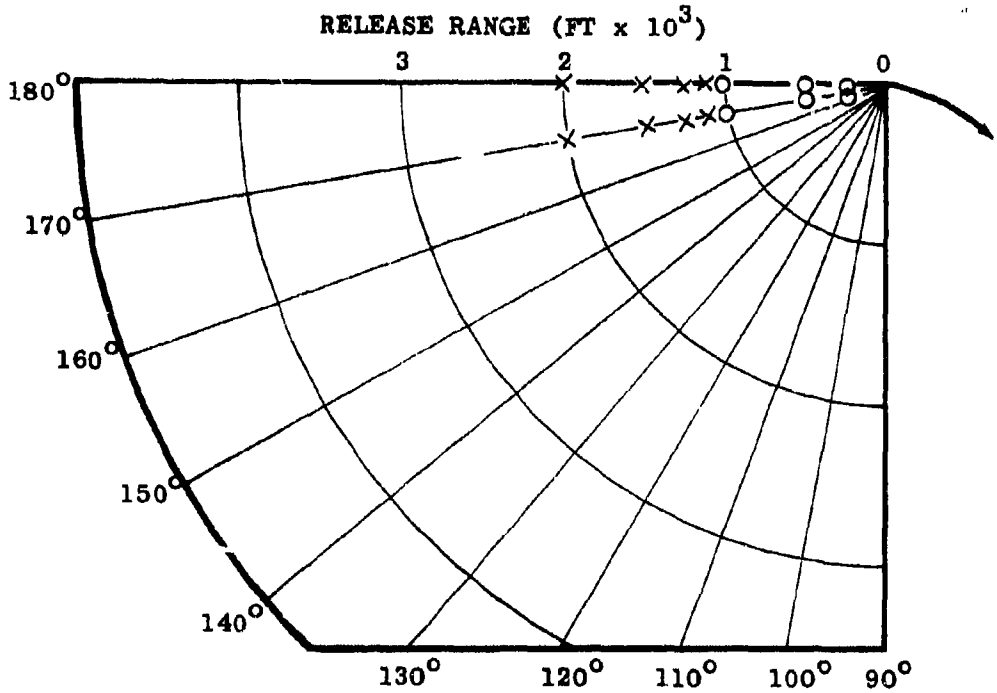


FIG. 27 - FLARE SUCCESS VERSUS FLARE EJECTION TIME (S)

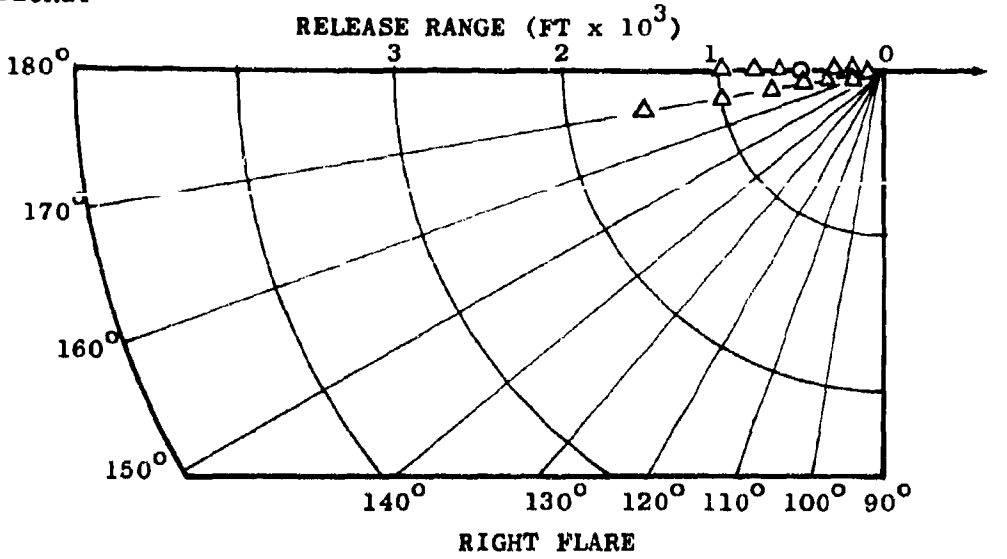


× DECOY SUCCESS
△ PREDETONATION SUCCESS
○ FLARE FAILURE

F-4B
ALTITUDE = 5,000 FT
LAUNCH RANGE = 3,000 FT
LAUNCH SPEED = M 0.9
TARGET SPEED = M 0.9
NO MANEUVER

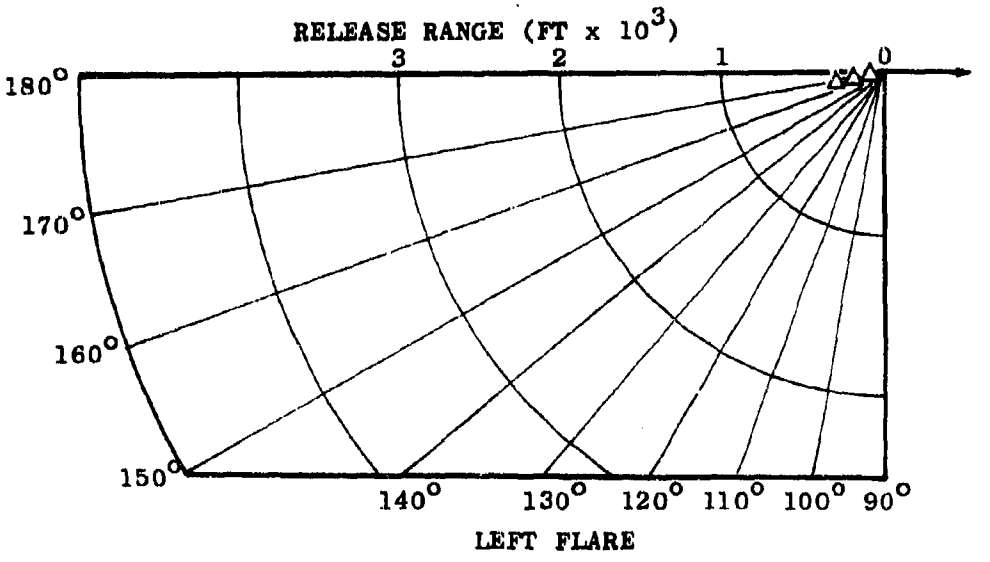


FIG. 28 - FLARE SUCCESS VERSUS FLARE EJECTION TIME (S)

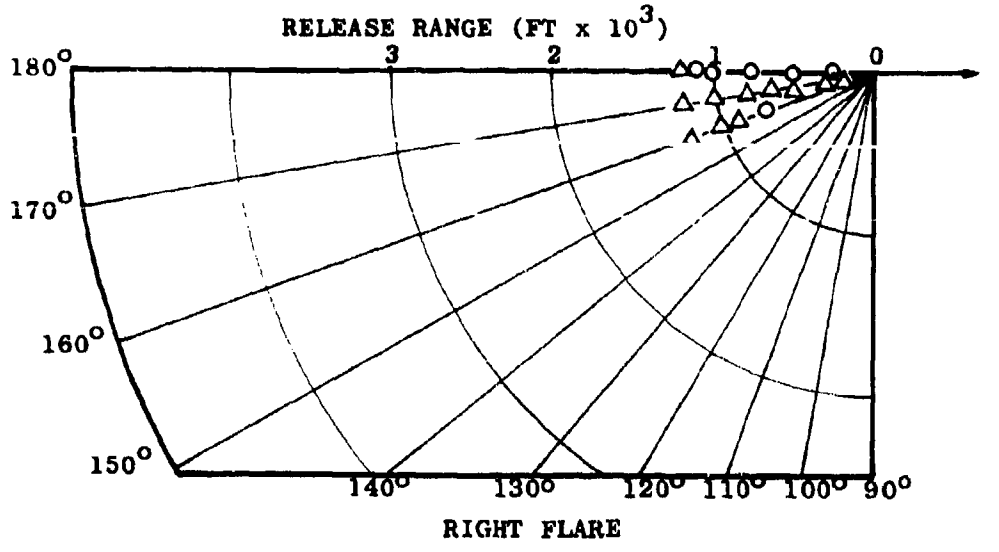


× DECOY SUCCESS
△ PREDETONATION SUCCESS
○ FLARE FAILURE

F-4B
ALTITUDE = 5,000 FT
LAUNCH RANGE = 5,000 FT
LAUNCH SPEED = M 0.9
TARGET SPEED = M 0.9
NO MANEUVER

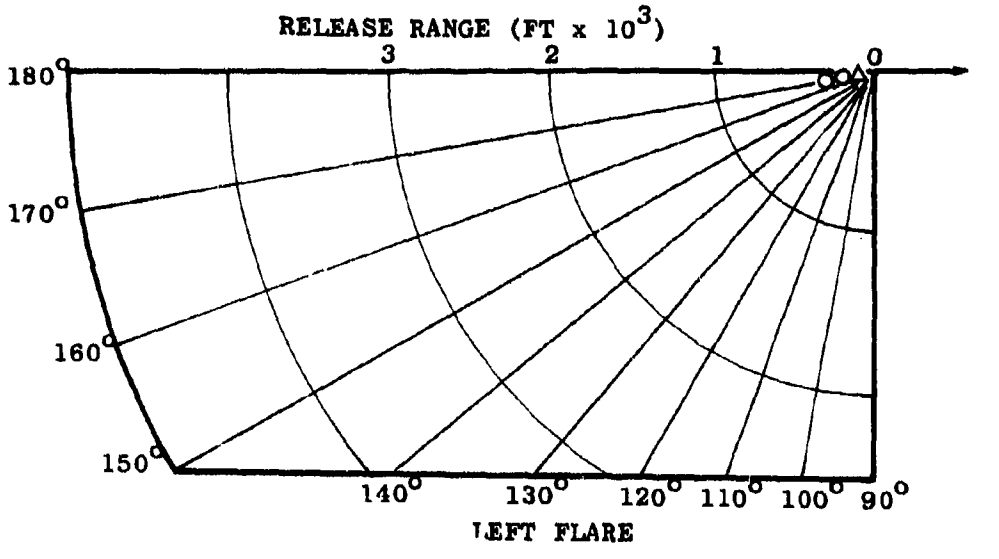


FIG. 29 - FLARE SUCCESS VERSUS FLARE EJECTION TIME (S)

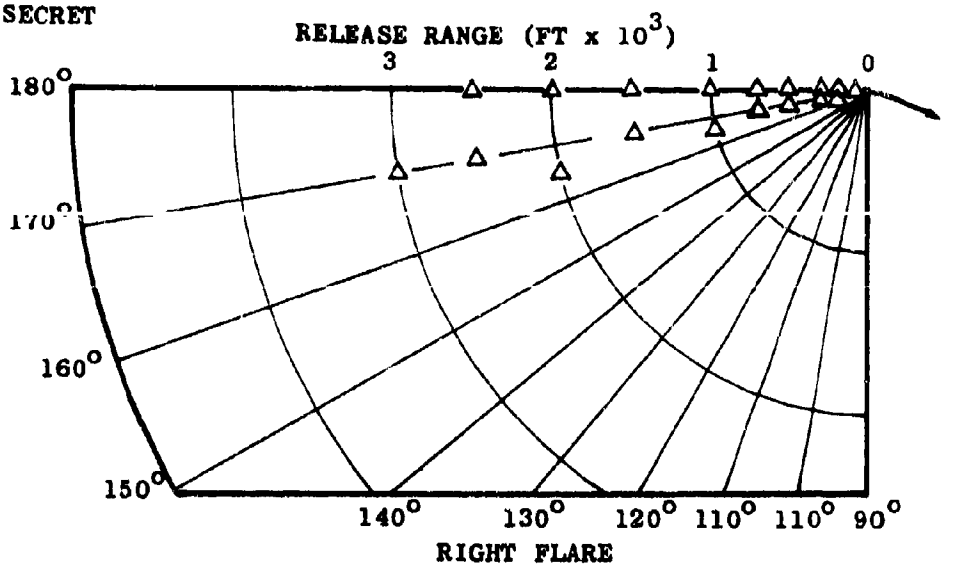


× DECOY SUCCESS
△ PREDETONATION SUCCESS
○ FLARE FAILURE

F-4B
ALTITUDE = 5,000 FT
LAUNCH RANGE = 3,000 FT
LAUNCH SPEED = M 0.9
TARGET SPEED = M 0.9
3g TURN

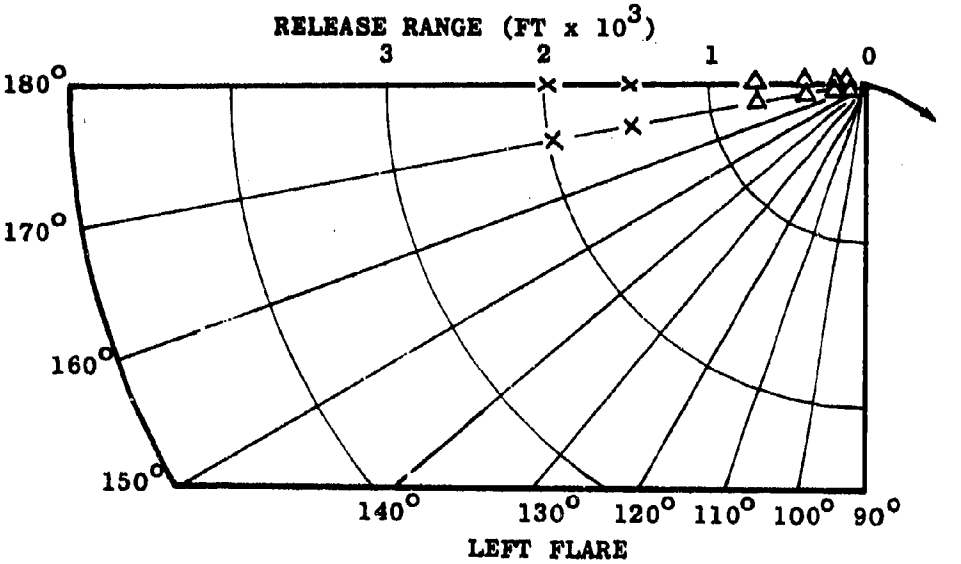


FIG. 30 - FLARE SUCCESS VERSUS FLARE EJECTION TIME (S)

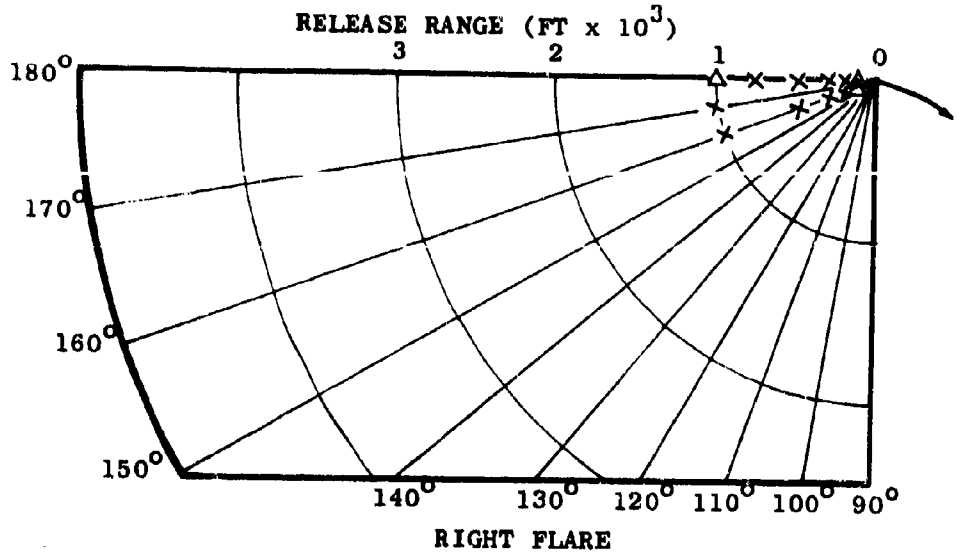


× DECOY SUCCESS
△ PREDETONATION SUCCESS
○ FLARE FAILURE

F-4B
ALTITUDE = 5,000 FT
LAUNCH RANGE = 5,000 FT
LAUNCH SPEED = M 0.9
TARGET SPEED = M 0.9
3g TURN

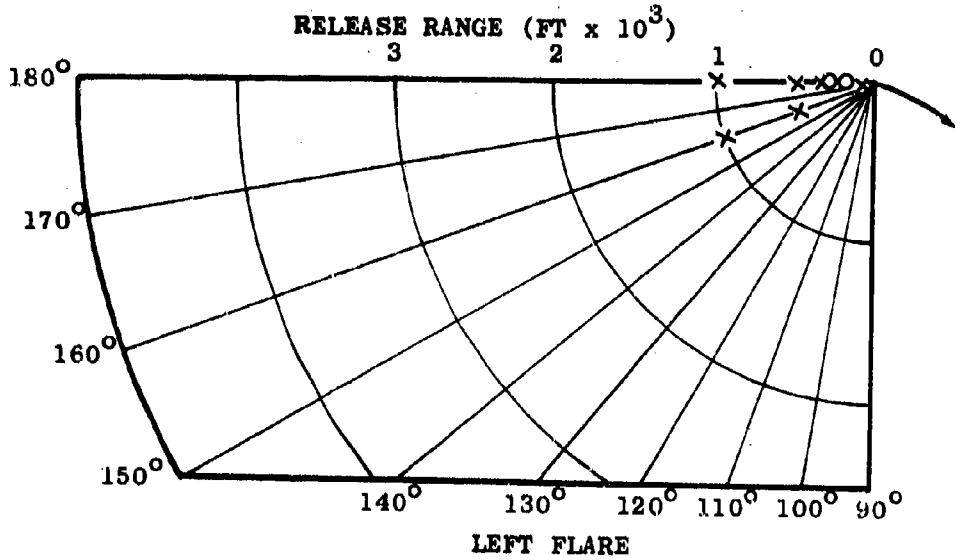


FIG. 31 - FLARE SUCCESS VERSUS FLARE EJECTION TIME (S)

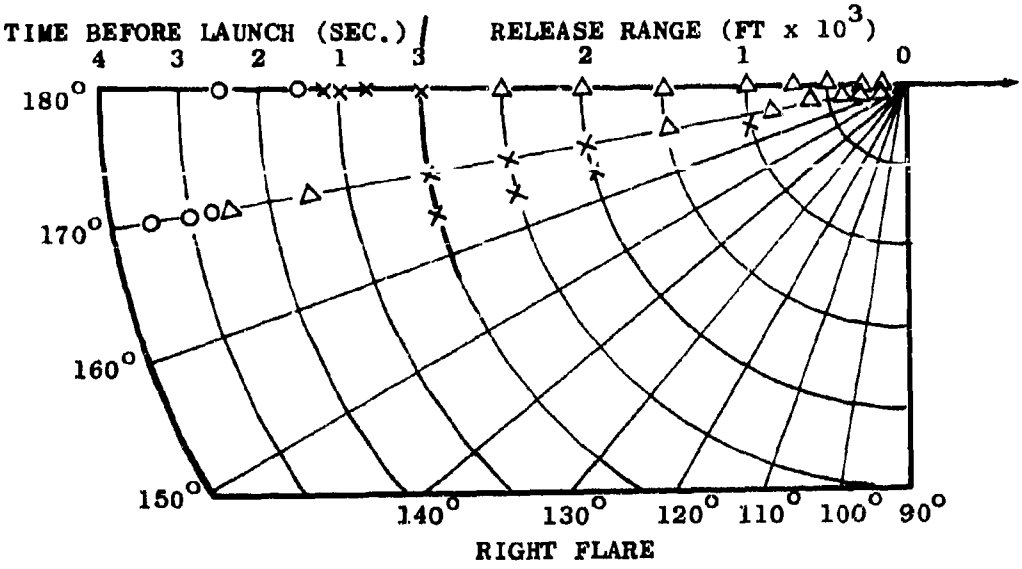


RIGHT FLARE

× DECOY SUCCESS
△ PREDETONATION SUCCESS
○ FLARE FAILURE

F-4B
ALTITUDE = 15,000 FT
LAUNCH RANGE = 3,000 FT
LAUNCH SPEED = M 1.2
TARGET SPEED = M 0.9
NO MANEUVER

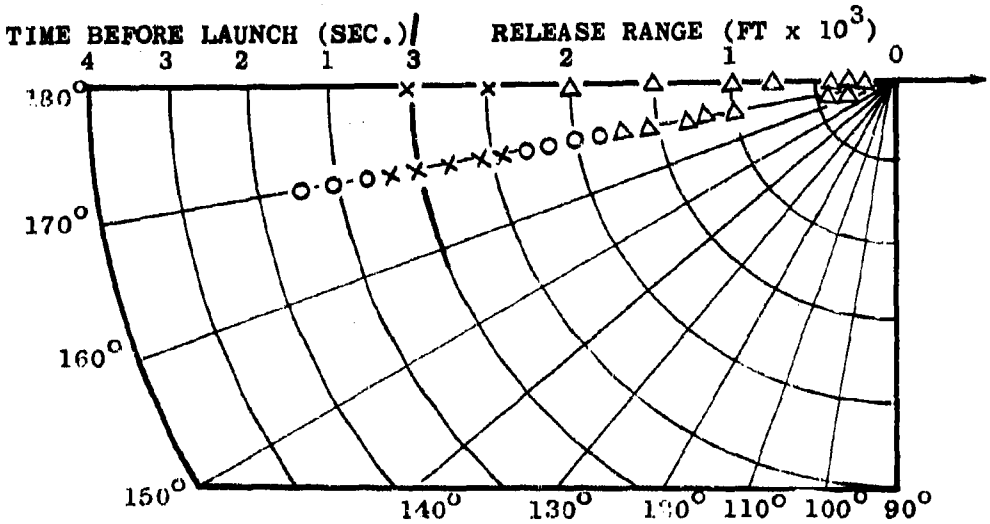


LEFT FLARE

FIG. 32 - FLARE SUCCESS VERSUS FLARE EJECTION TIME (S)

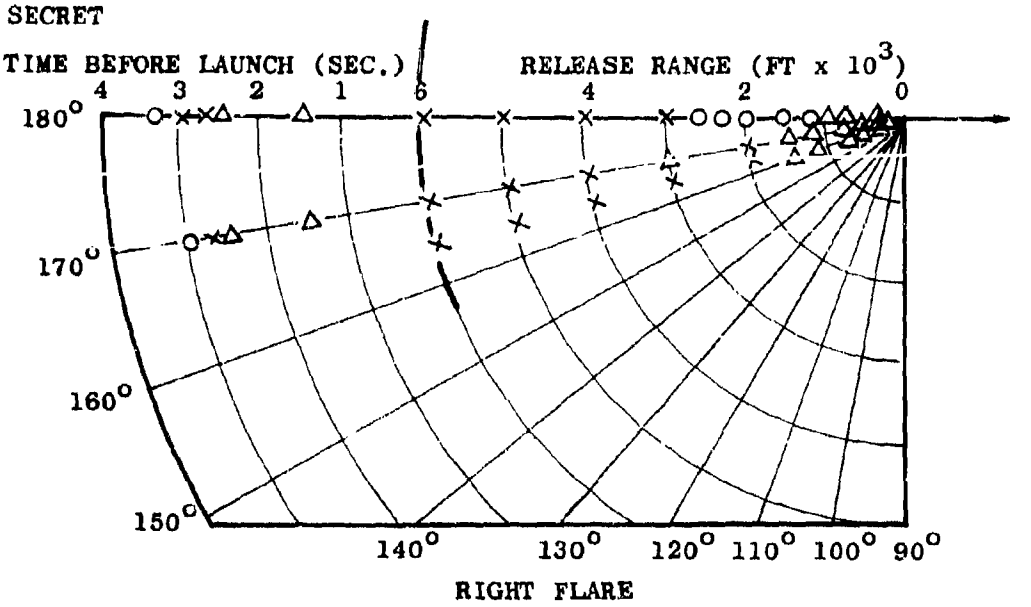


× DECOY SUCCESS
△ PREDETONATION SUCCESS
○ FLARE FAILURE

F-4B
ALTITUDE - 15,000 FT
LAUNCH RANGE - 6,000 FT
LAUNCH SPEED - M 1.2
TARGET SPEED - M 0.9
NO MANEUVER

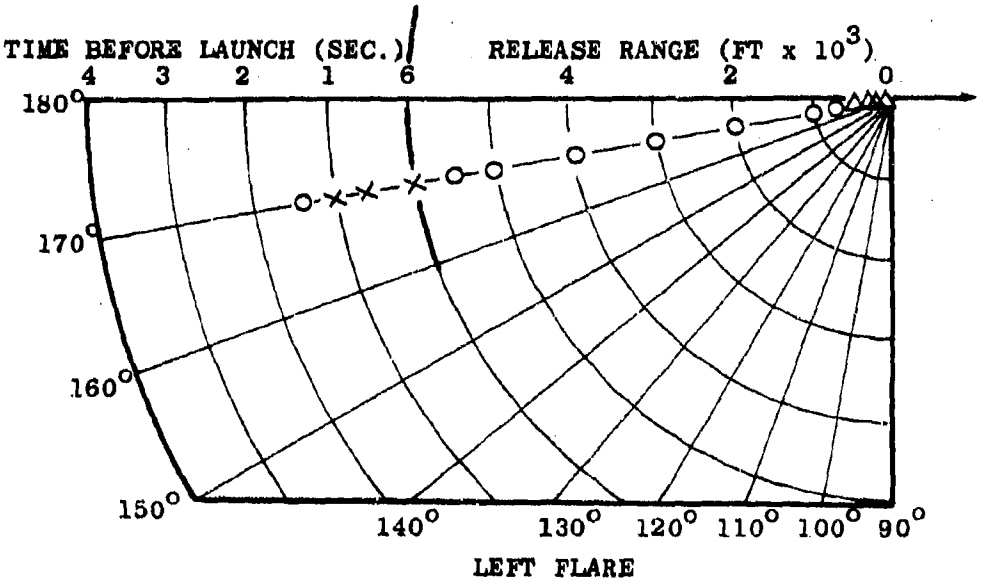


FIG. 33 - FLARE SUCCESS VERSUS FLARE EJECTION TIME (S)

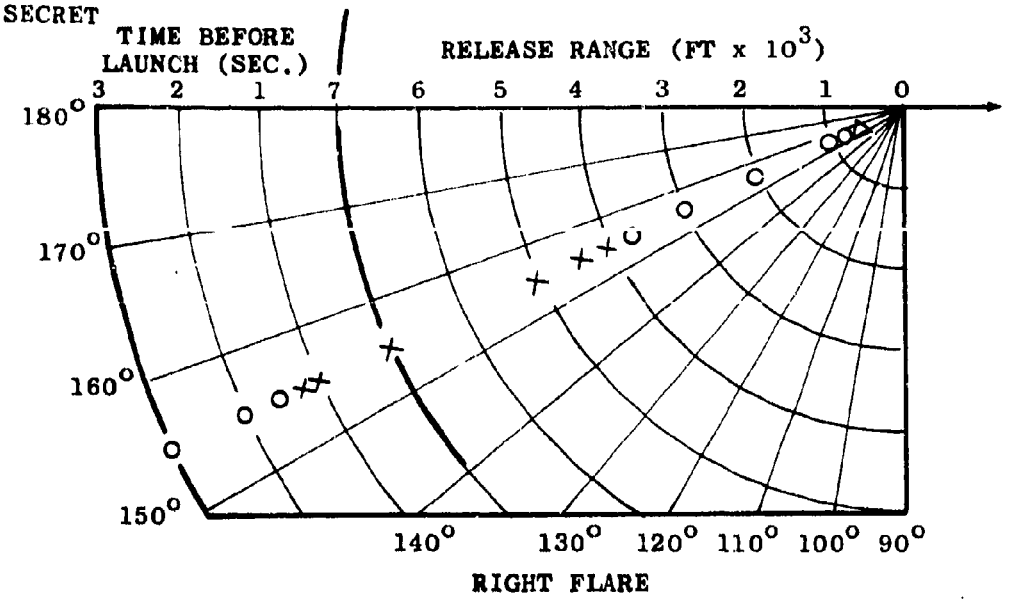


× DECOY SUCCESS
△ PREDETONATION SUCCESS
○ FLARE FAILURE

F-4B
ALTITUDE = 15,000 FT
LAUNCH RANGE = 7,000 FT
LAUNCH SPEED = M 1.2
TARGET SPEED = M 0.9
NO MANEUVER

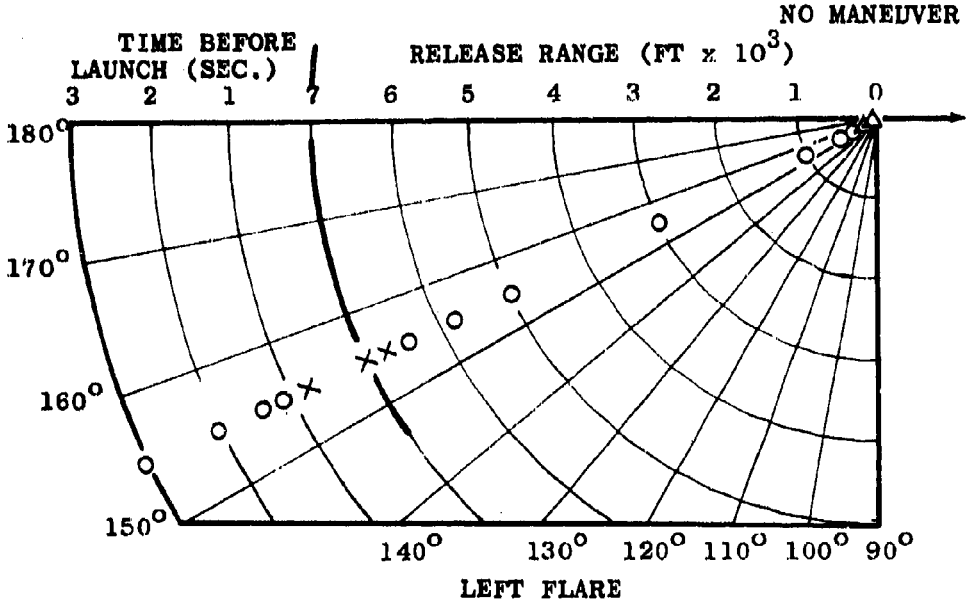


FIG. 34 - FLARE SUCCESS VERSUS FLARE EJECTION TIME (S)

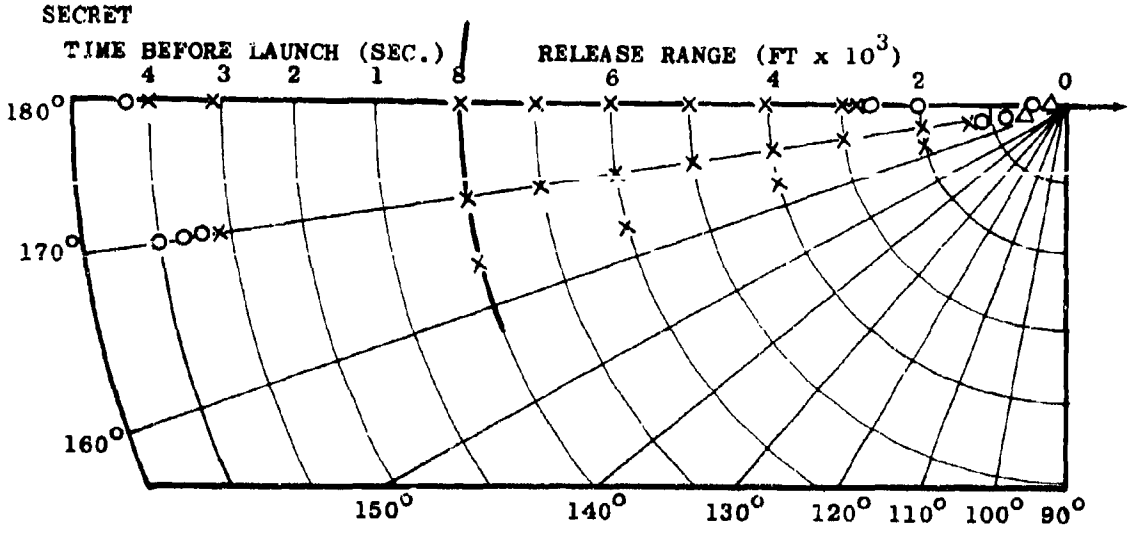


RIGHT FLARE

× DECOY SUCCESS
△ PREDETONATION SUCCESS
○ FLARE FAILURE

F-4B
ALTITUDE = 15,000 FT
LAUNCH RANGE = 8,000 FT
LAUNCH SPEED = M 1.2
TARGET SPEED = M 0.9
NO MANEUVER

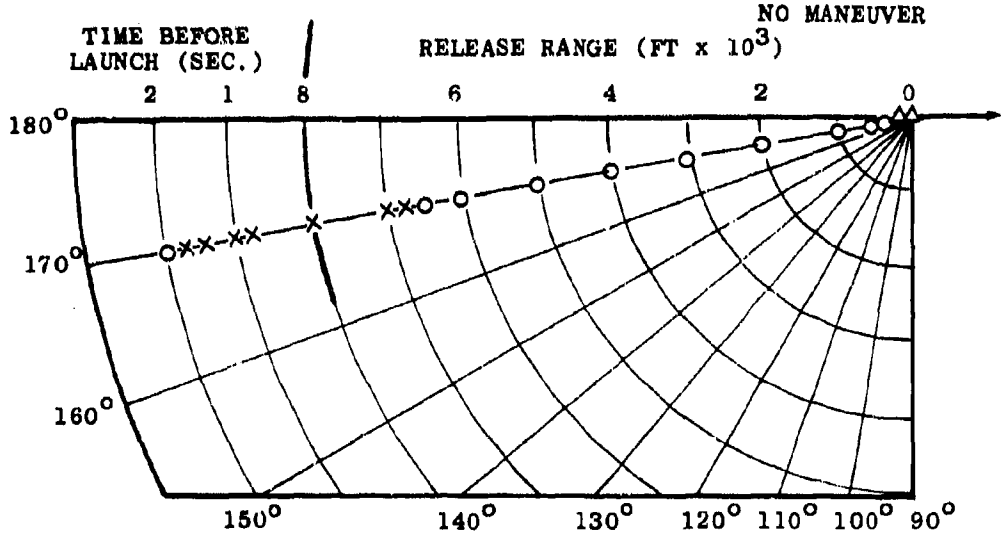


LEFT FLARE

FIG. 35 - FLARE SUCCESS VERSUS FLARE EJECTION TIME (S)

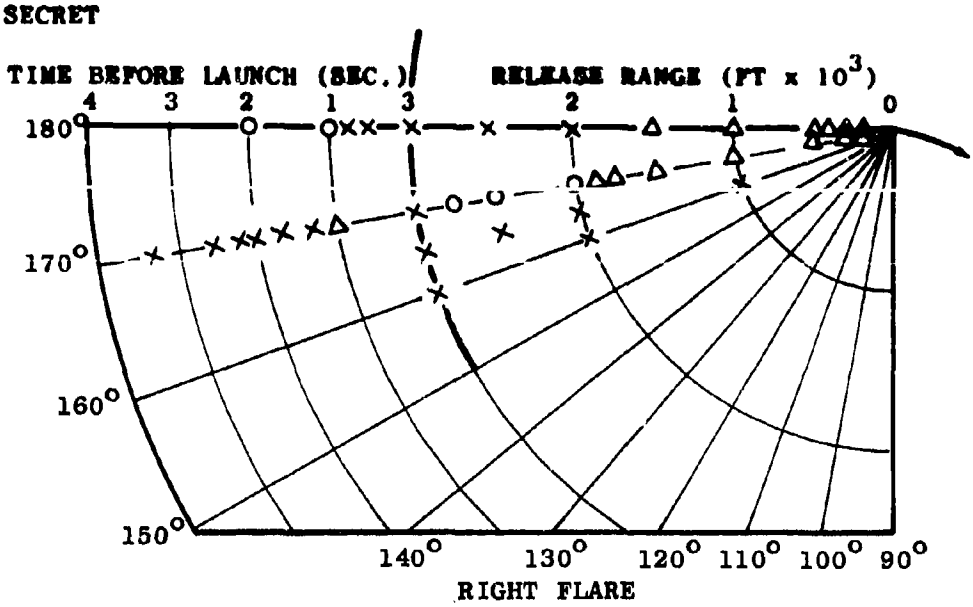


× DECOY SUCCESS
△ PREDETONATION SUCCESS
○ FLARE FAILURE

F-4B
ALTITUDE = 15,000 FT
LAUNCH RANGE = 3,000 FT
LAUNCH SPEED = M 1.2
TARGET SPEED = M 0.9
3g TURN

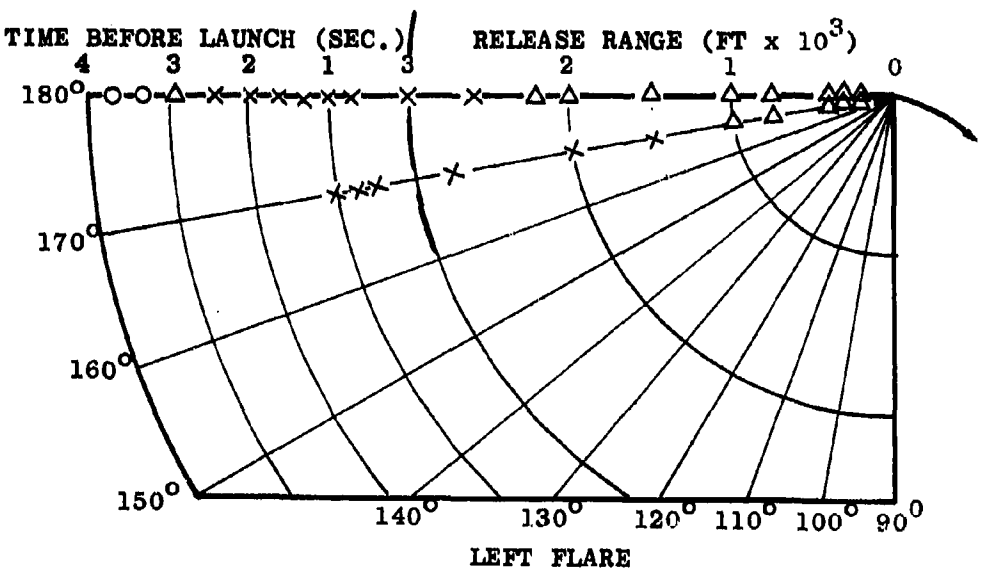


FIG. 36 - FLARE SUCCESS VERSUS FLARE EJECTION TIME (S)

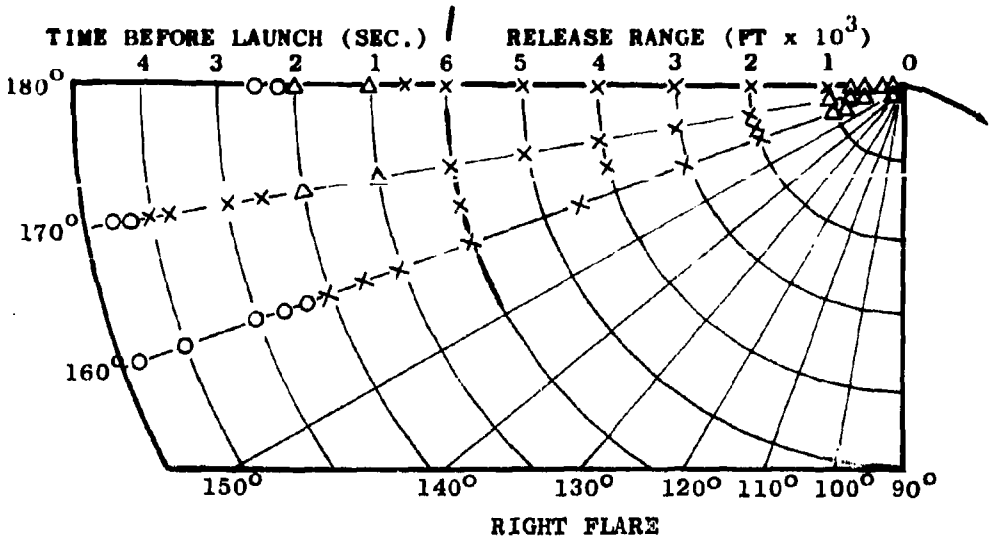


× DECOY SUCCESS
△ PREDETONATION SUCCESS
○ FLARE FAILURE

F-4B
ALTITUDE = 15,000 FT
LAUNCH RANGE = 6,000 FT
LAUNCH SPEED = M 1.2
TARGET SPEED = M 0.9
3g TURN

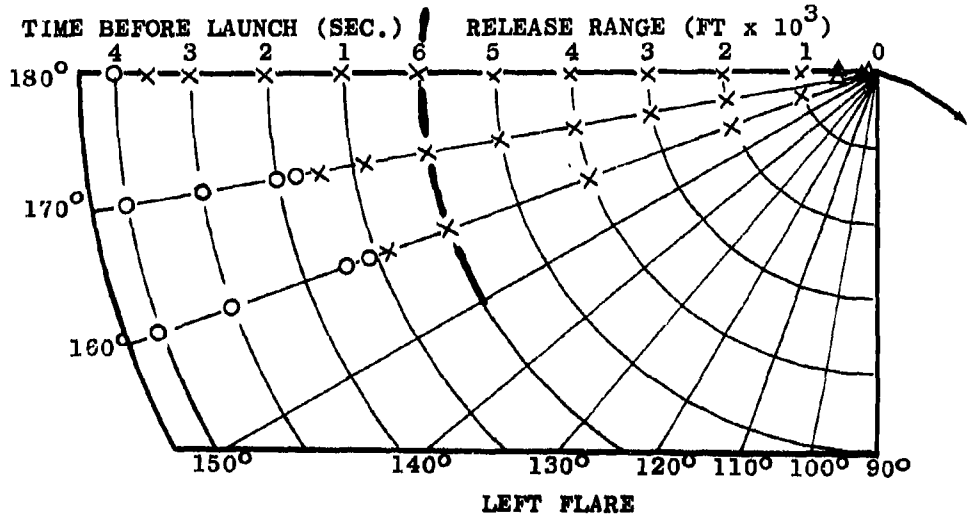


FIG. 37 - FLARE SUCCESS VERSUS FLARE EJECTION TIME (S)

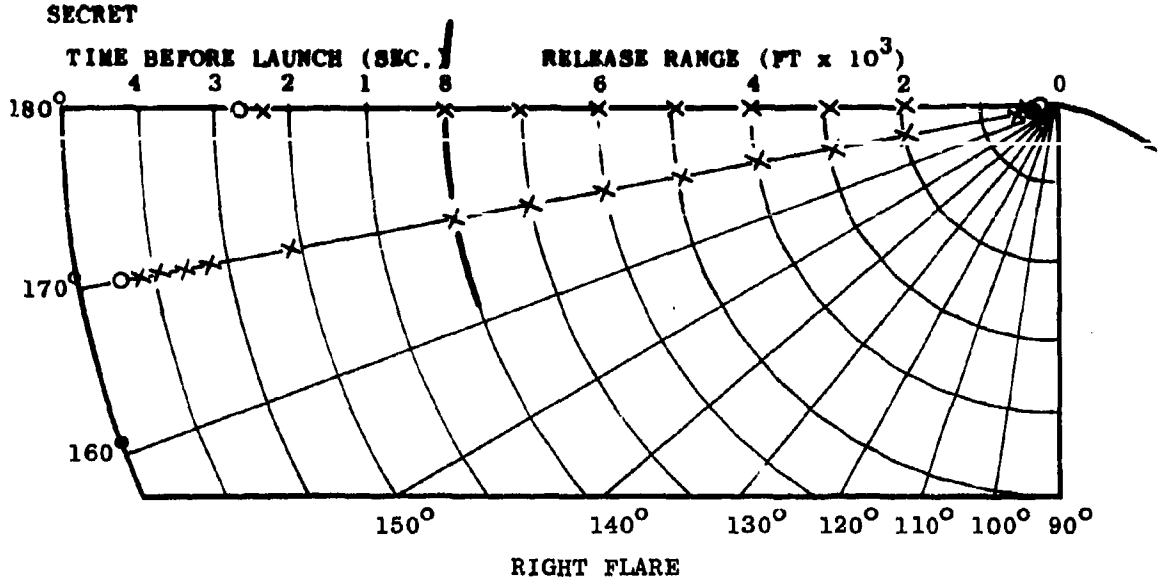


RIGHT FLARE

× DECOY SUCCESS
△ PREDETONATION SUCCESS
○ FLARE FAILURE

F-4B
ALTITUDE = 15,000 FT
LAUNCH RANGE = 8,000 FT
LAUNCH SPEED = M 1.2
TARGET SPEED = M 0.9
3g TURN

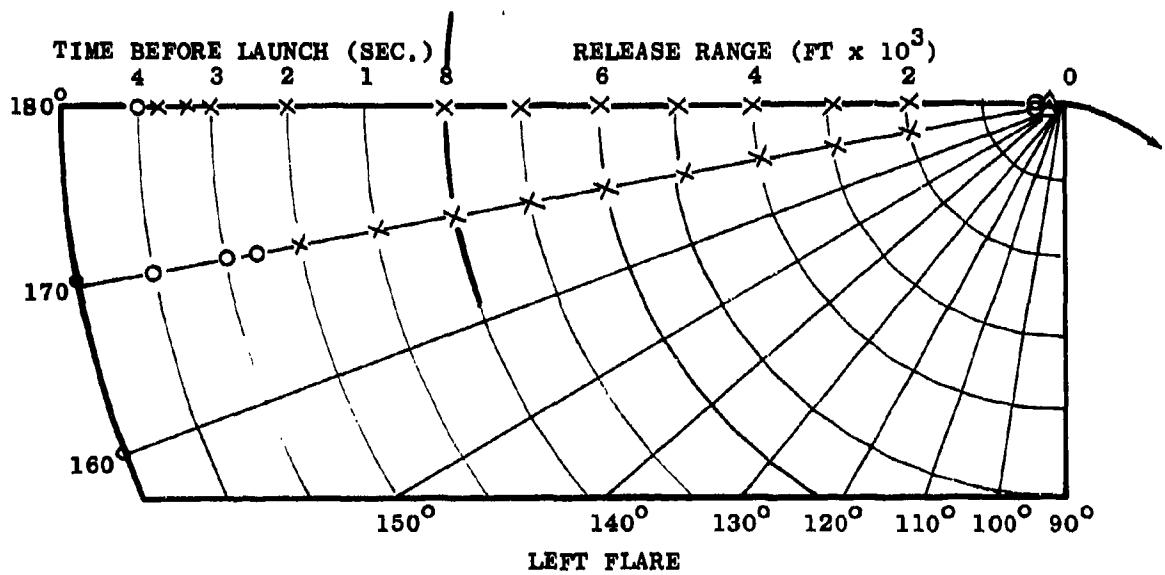


LEFT FLARE

FIG. 38 - FLARE SUCCESS VERSUS FLARE EJECTION TIME (S)

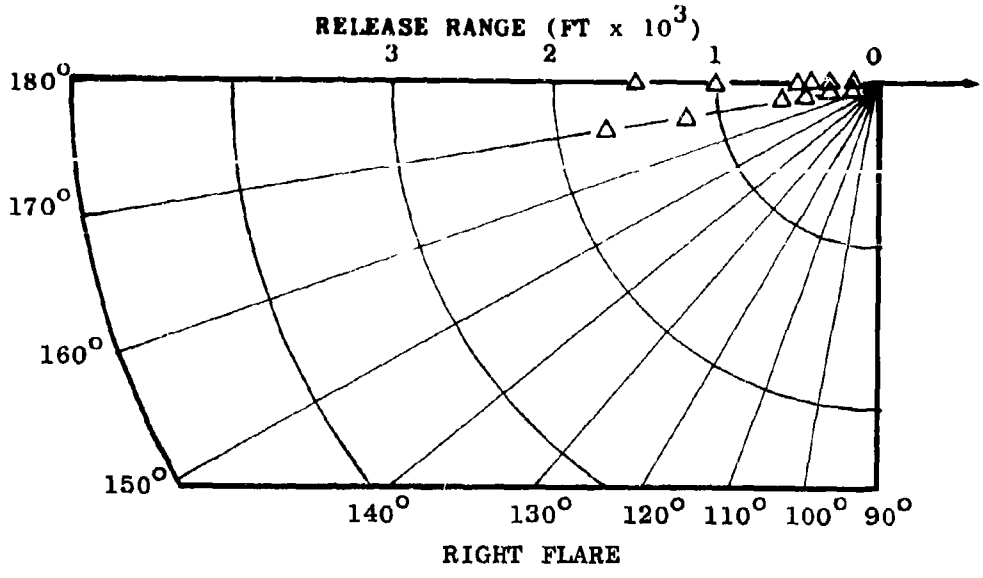


× DECOY SUCCESS
△ PREDETONATION SUCCESS
○ FLARE FAILURE

F-4B
ALTITUDE = 30,000 FT
LAUNCH RANGE = 4,000 FT
LAUNCH SPEED = M 1.2
TARGET SPEED = M 0.9
NO MANEUVER

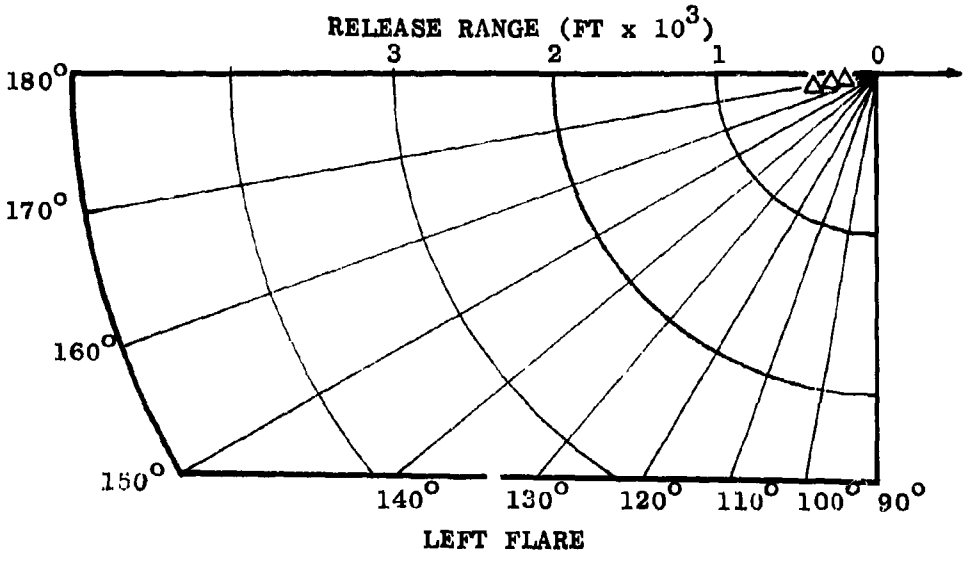


FIG. 39 - FLARE SUCCESS VERSUS FLARE EJECTION TIME (S)

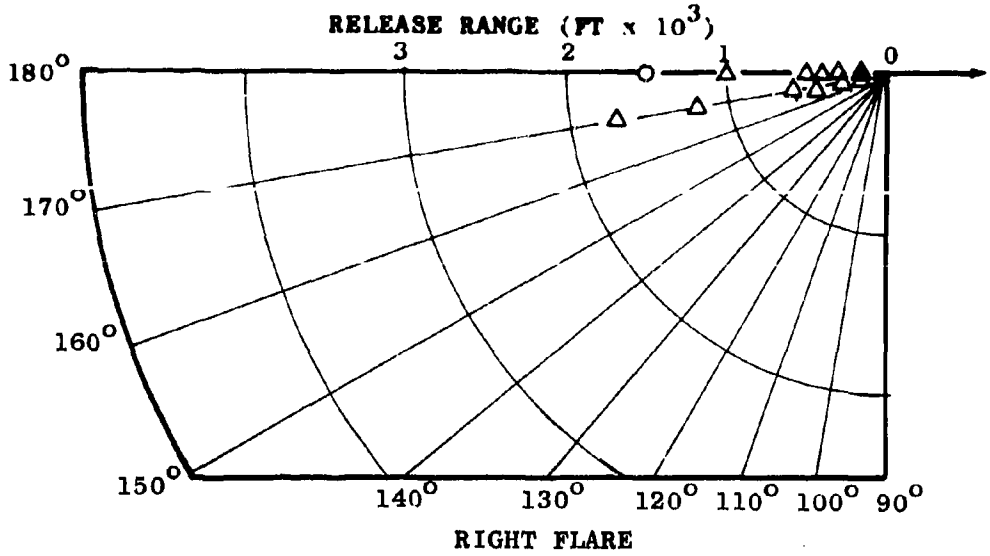


× DECOY SUCCESS
△ PREDETONATION SUCCESS
○ FLARE FAILURE

F-4B
ALTITUDE = 30,000 FT
LAUNCH RANGE = 8,000 FT
LAUNCH SPEED = M 1.2
TARGET SPEED = M 0.9
NO MANEUVER

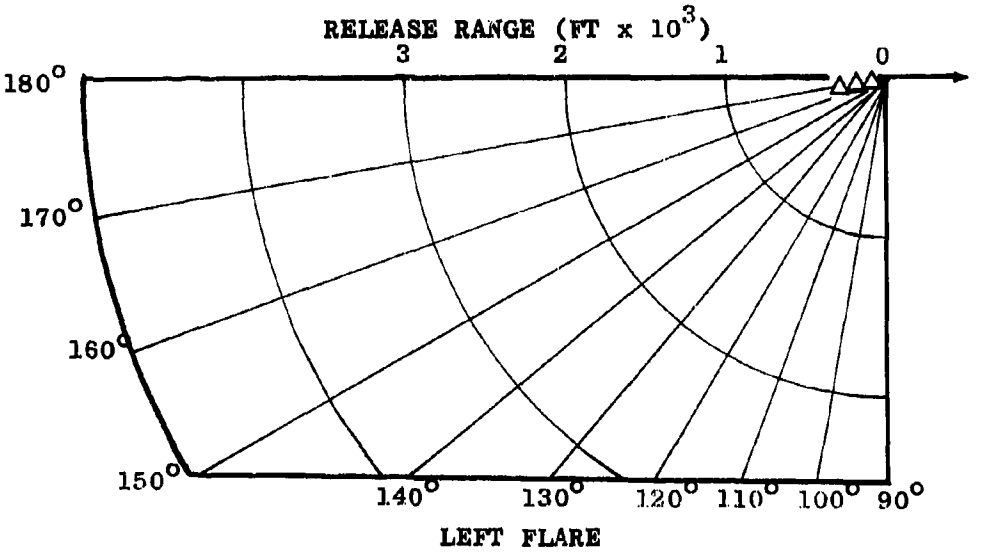


FIG. 40 - FLARE SUCCESS VERSUS FLARE EJECTION TIME (S)

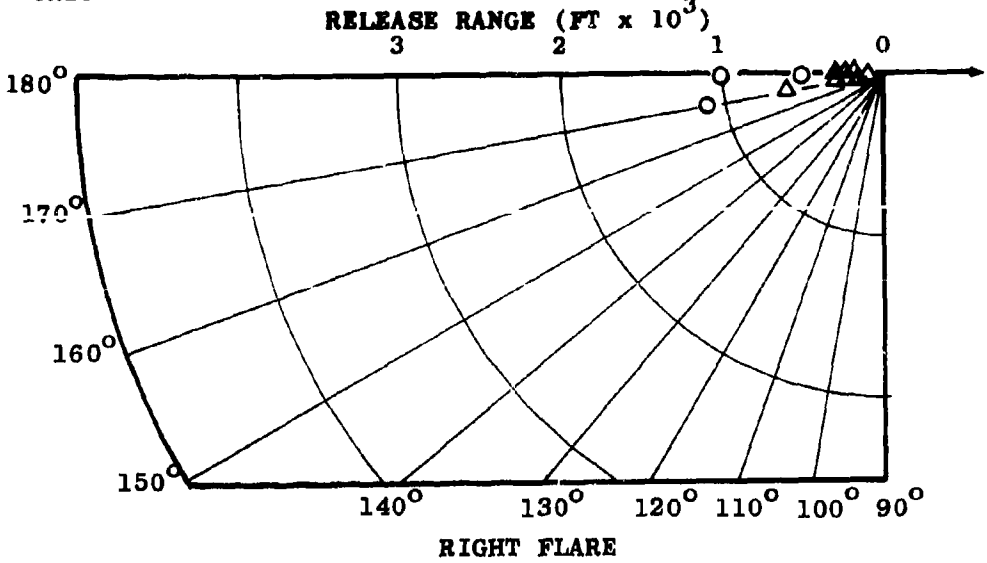


× DECOY SUCCESS
△ PREDETONATION SUCCESS
○ FLARE FAILURE

F-4B
ALTITUDE = 30,000 FT
LAUNCH RANGE = 12,000 FT
LAUNCH SPEED = M 1.2
TARGET SPEED = M 0.9
NO MANEUVER

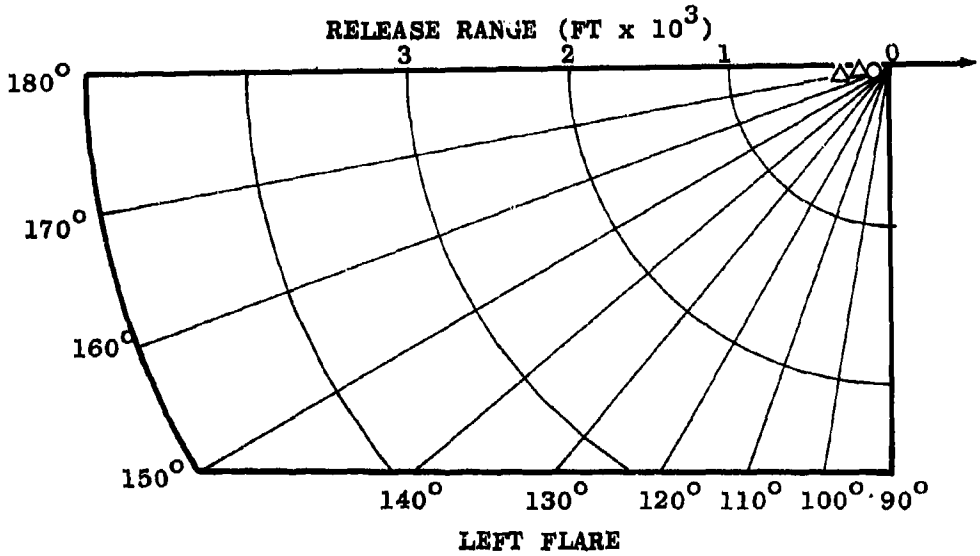


FIG. 41 - FLARE SUCCESS VERSUS FLARE EJECTION TIME (S)

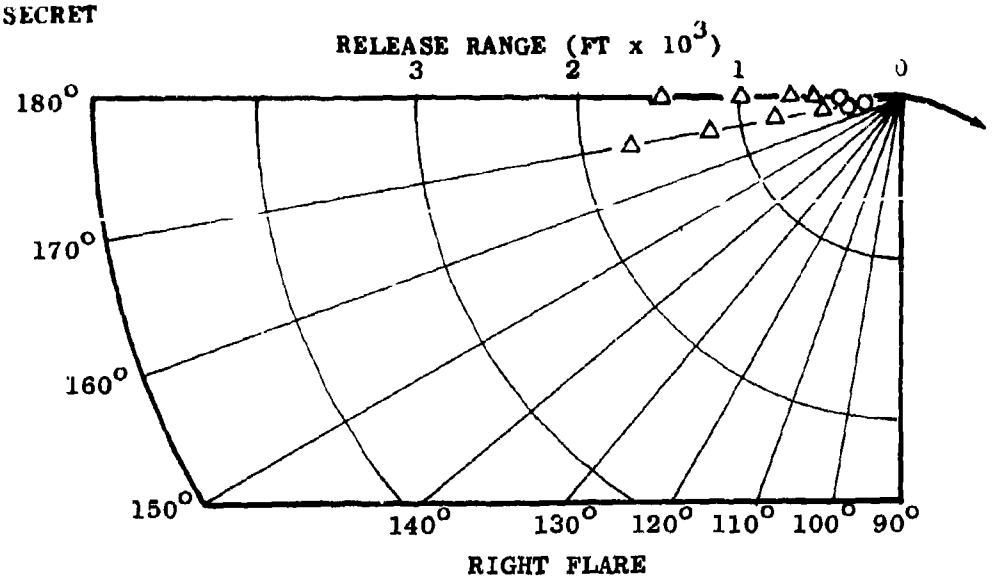


× DECOY SUCCESS
△ PREDETONATION SUCCESS
○ FLARE FAILURE

F-4B
ALTITUDE = 30,000 FT
LAUNCH RANGE = 4,000 FT
LAUNCH SPEED = M 1.2
TARGET SPEED = M 0.9
3g TURN

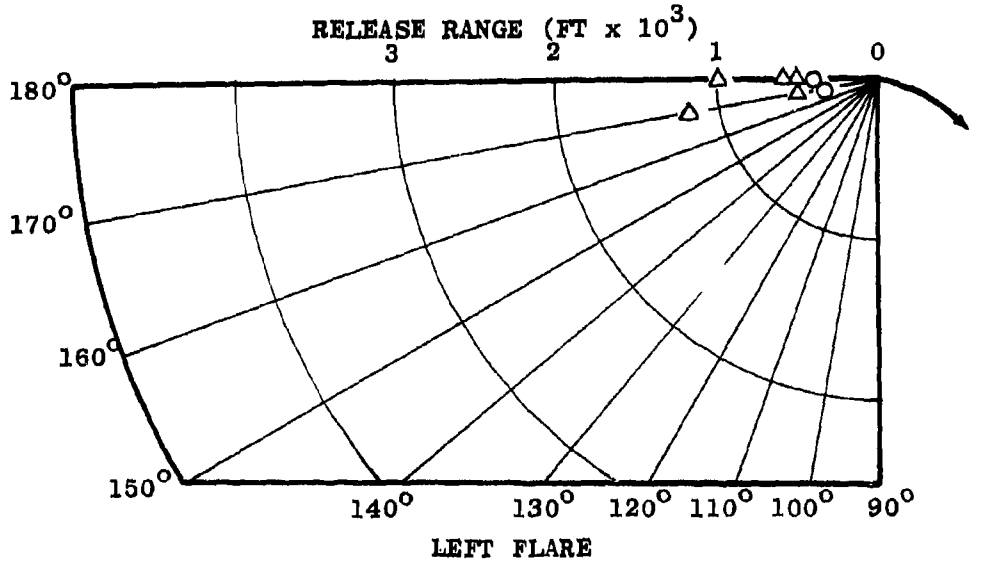


FIG. 42 - FLARE SUCCESS VERSUS FLARE EJECTION TIME (S)

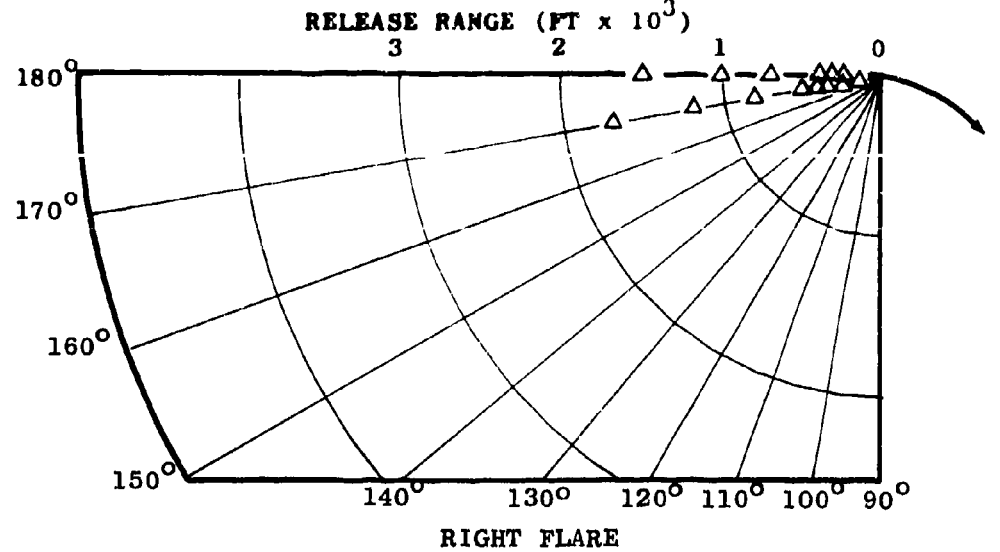


× DECOY SUCCESS
△ PREDETONATION SUCCESS
○ FLARE FAILURE

F-4B
ALTITUDE = 30,000 FT
LAUNCH RANGE = 8,000 FT
LAUNCH SPEED = M 1.2
TARGET SPEED = M 0.9
3g TURN

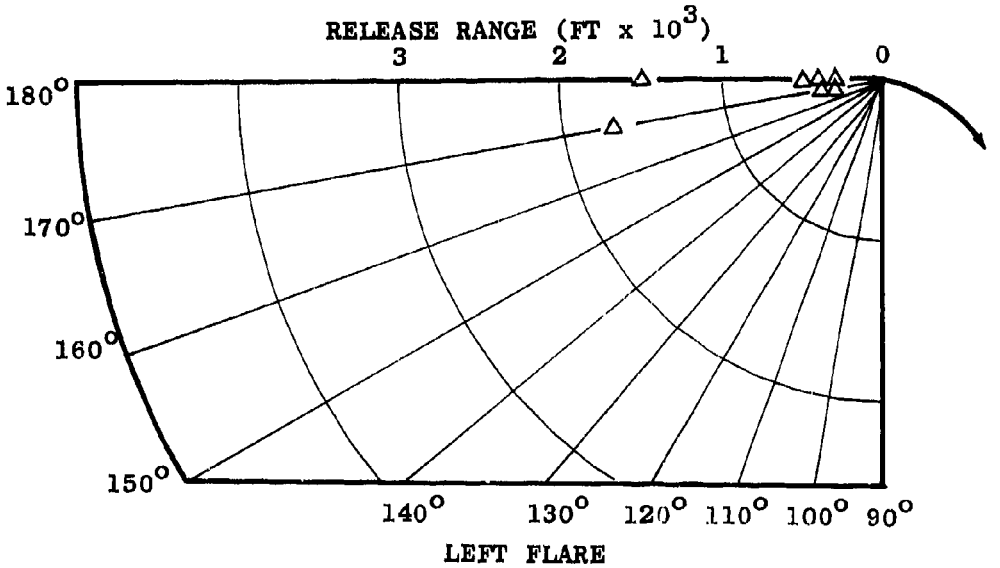


FIG. 43 - FLARE SUCCESS VERSUS FLARE EJECTION TIME (S)

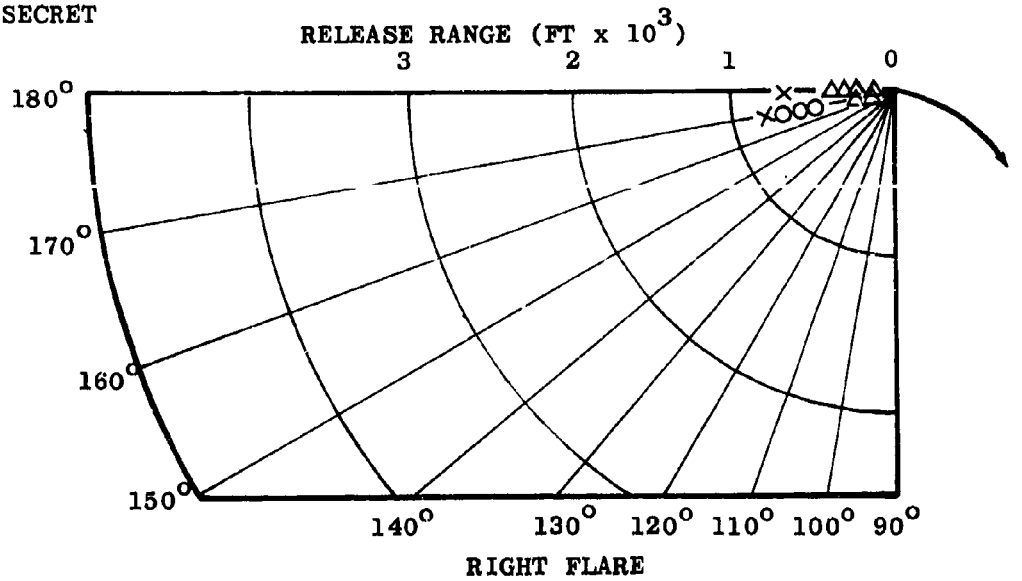


× DECOY SUCCESS
△ PREDETONATION SUCCESS
○ FLARE FAILURE

F-4B
ALTITUDE = 30,000 FT
LAUNCH RANGE = 12,000 FT
LAUNCH SPEED = M 1.2
TARGET SPEED = M 0.9
3g TURN

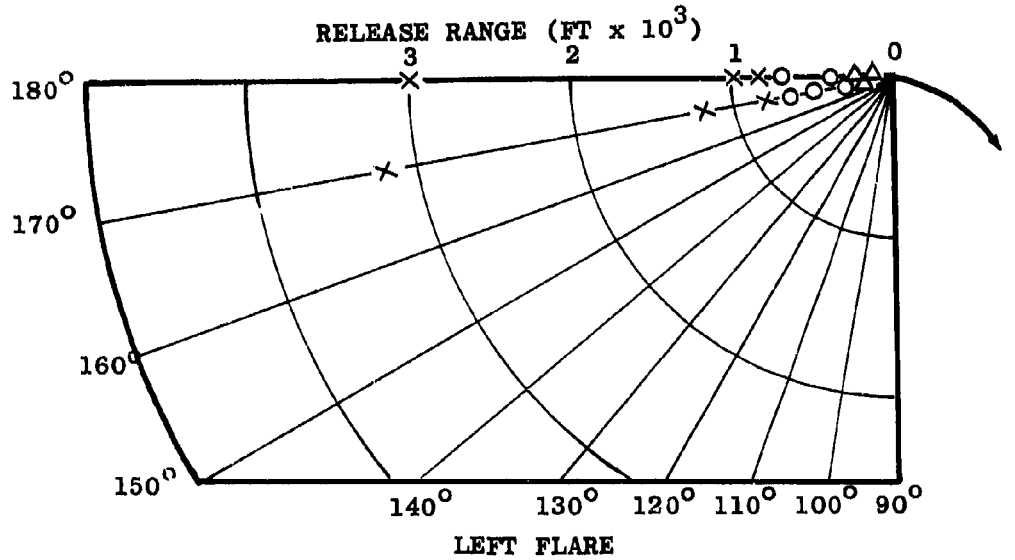


FIG. 44 - FLARE SUCCESS VERSUS FLARE EJECTION TIME (S)

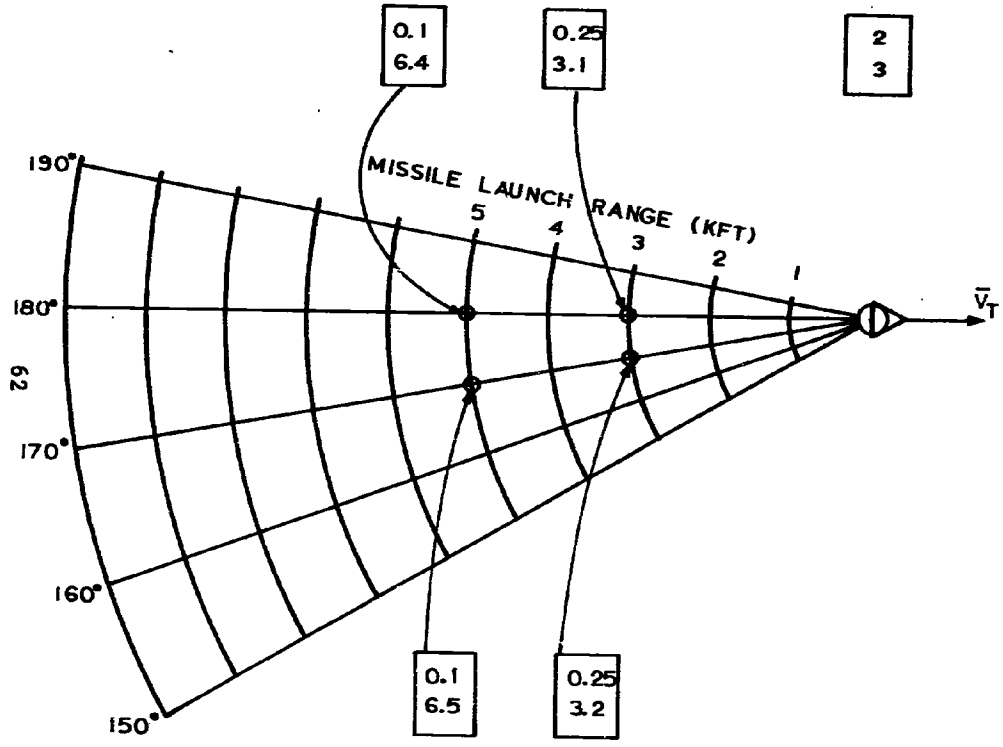


62



FIG. 45 - FLARE EFFECTIVENESS SUMMARY (S)

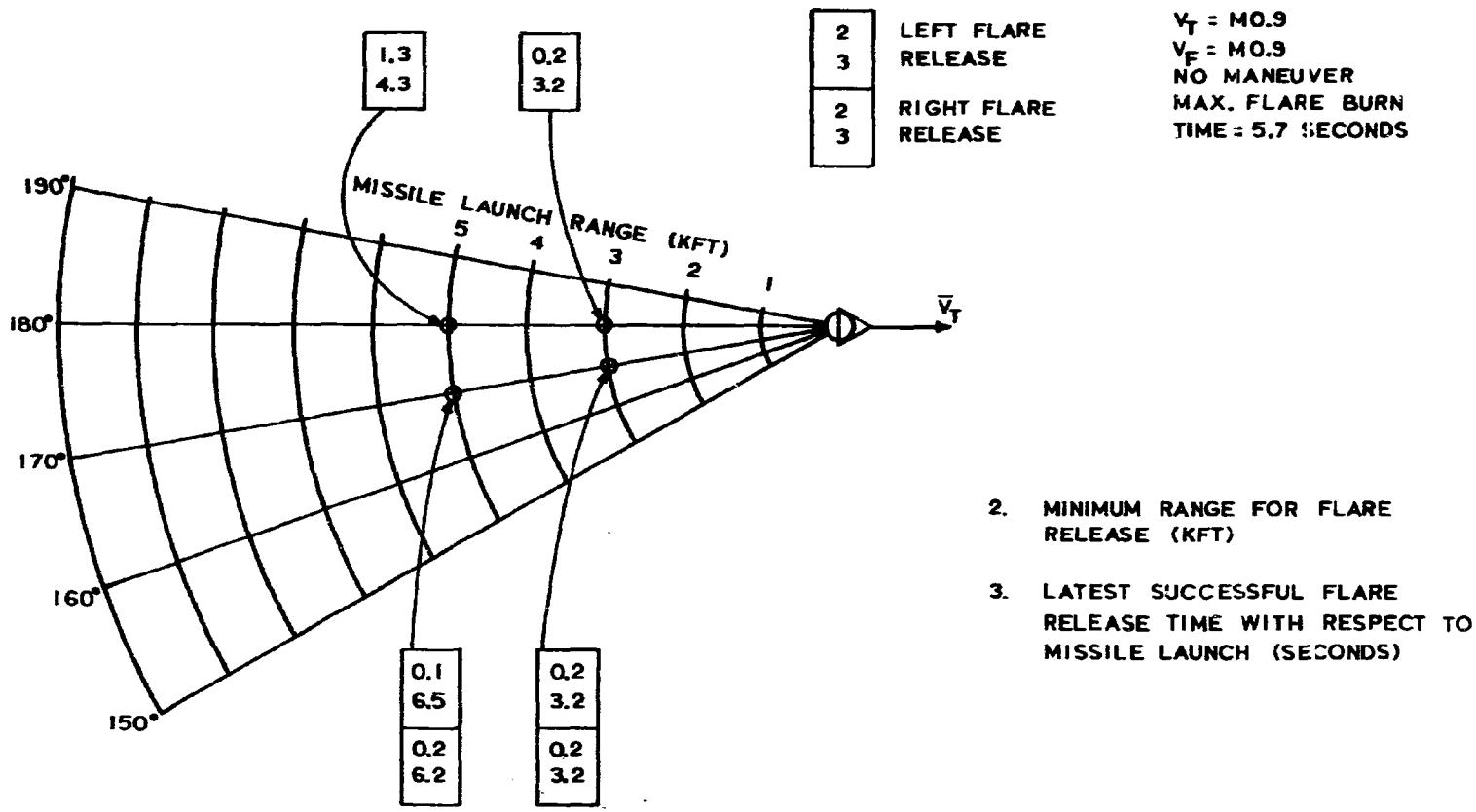


FIG. 46 - FLARE EFFECTIVENESS SUMMARY (S)

F-8
ALT = 5 KFT
$V_T$ = M0.9
$V_F$ = M0.9
3g TURN
MAX. FLARE BURN
TIME = 5.7 SECONDS

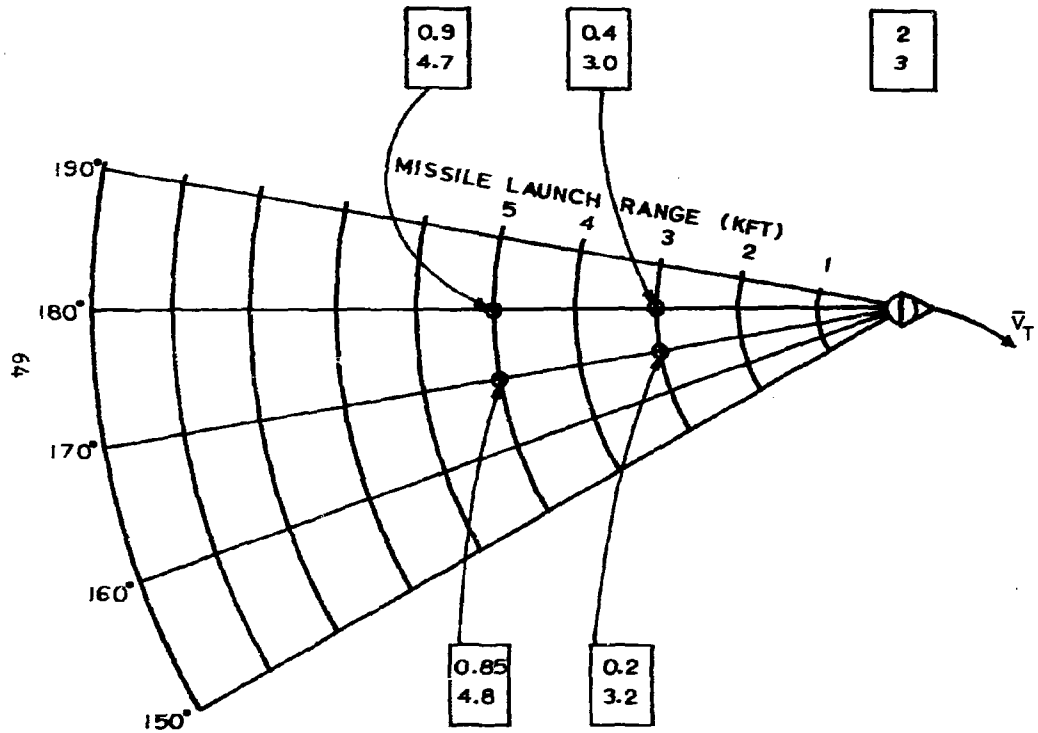


2. MINIMUM RANGE FOR FLARE RELEASE (KFT)

3. LATEST SUCCESSFUL FLARE RELEASE TIME WITH RESPECT TO MISSILE LAUNCH (SECONDS)

64



FIG. 47 - FLARE EFFECTIVENESS SUMMARY (S)

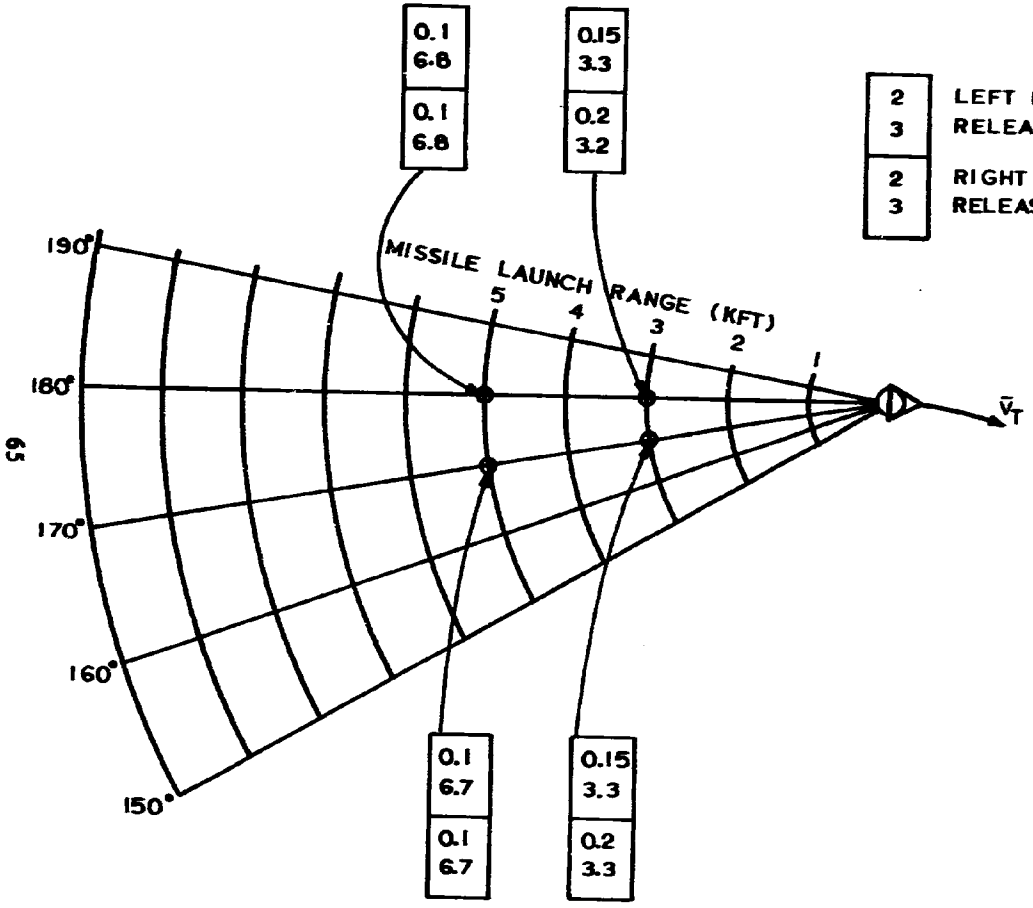


2. MINIMUM RANGE FOR FLARE RELEASE (KFT)

3. LATEST SUCCESSFUL FLARE RELEASE TIME WITH RESPECT TO MISSILE LAUNCH (SECONDS)





FIG. 48 - FLARE EFFECTIVENESS SUMMARY (S)

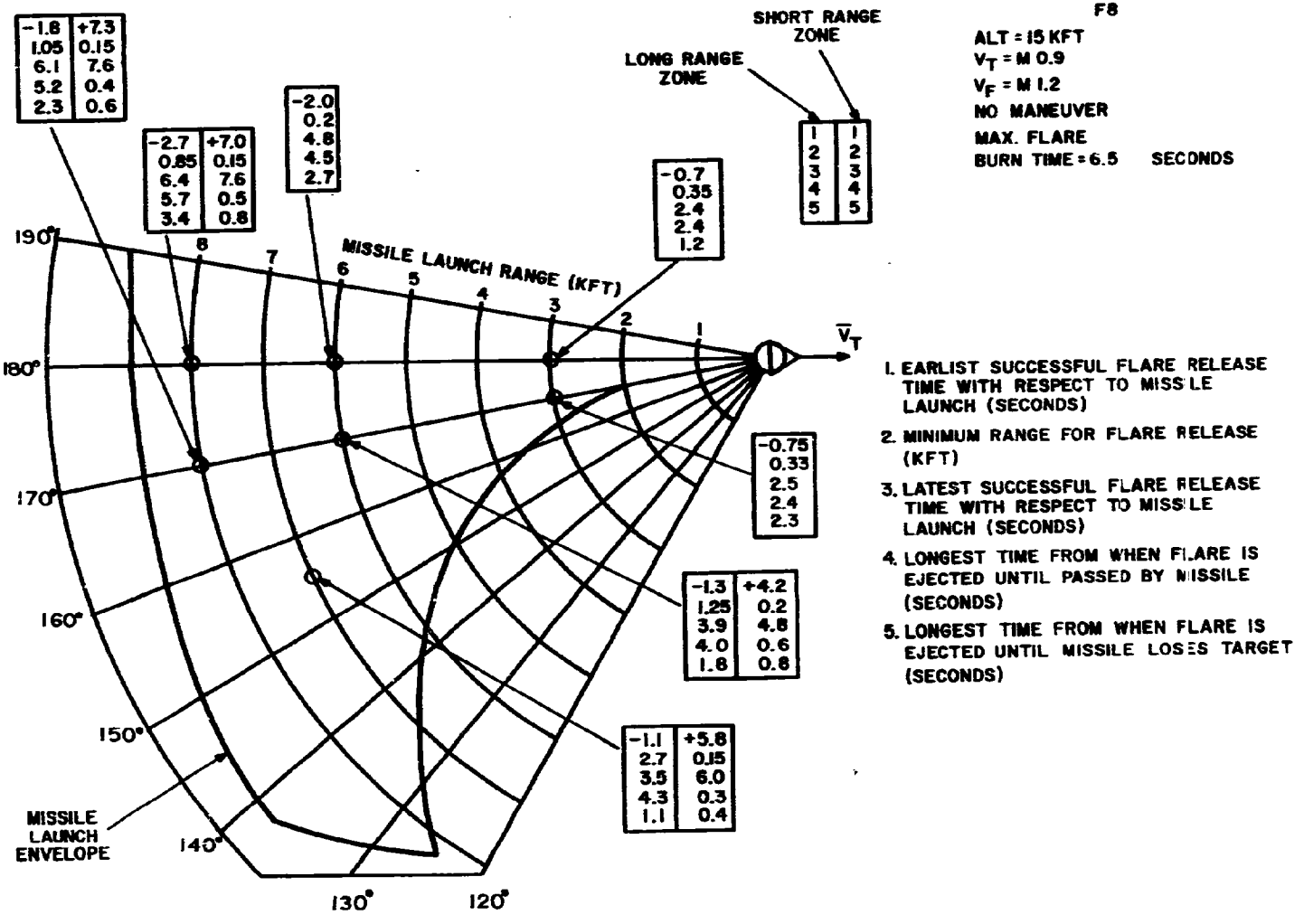


| | |
|---|---|
| -1.8 | +7.3 |
| 1.05 | 0.15 |
| 6.1 | 7.6 |
| 5.2 | 0.4 |
| 2.3 | 0.6 |

| | |
|---|---|
| -2.7 | +7.0 |
| 0.85 | 0.15 |
| 6.4 | 7.6 |
| 5.7 | 0.5 |
| 3.4 | 0.8 |

| |
|---|
| -2.0 |
| 0.2 |
| 4.8 |
| 4.5 |
| 2.7 |

| |
|---|
| -0.7 |
| 0.35 |
| 2.4 |
| 2.4 |
| 1.2 |

| | |
|---|---|
| 1 | 1 |
| 2 | 2 |
| 3 | 3 |
| 4 | 4 |
| 5 | 5 |

| |
|---|
| -0.75 |
| 0.33 |
| 2.5 |
| 2.4 |
| 2.3 |

| | |
|---|---|
| -1.3 | +4.2 |
| 1.25 | 0.2 |
| 3.9 | 4.8 |
| 4.0 | 0.6 |
| 1.8 | 0.8 |

| | |
|---|---|
| -1.1 | +5.8 |
| 2.7 | 0.15 |
| 3.5 | 6.0 |
| 4.3 | 0.3 |
| 1.1 | 0.4 |

FIG. 49 - FLARE EFFECTIVENESS SUMMARY (S)

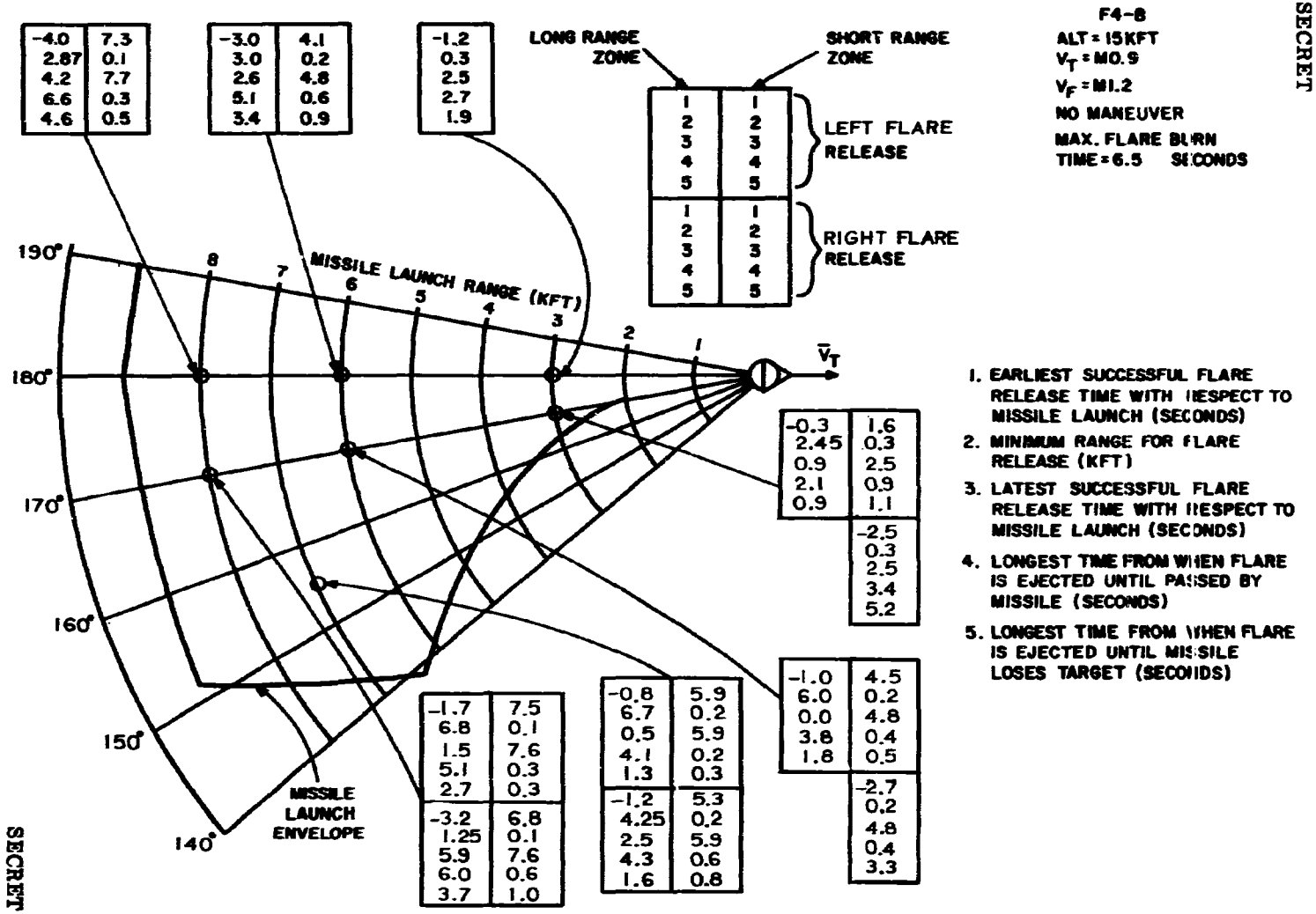


FIG. 50 - FLARE EFFECTIVENESS SUMMARY (S)

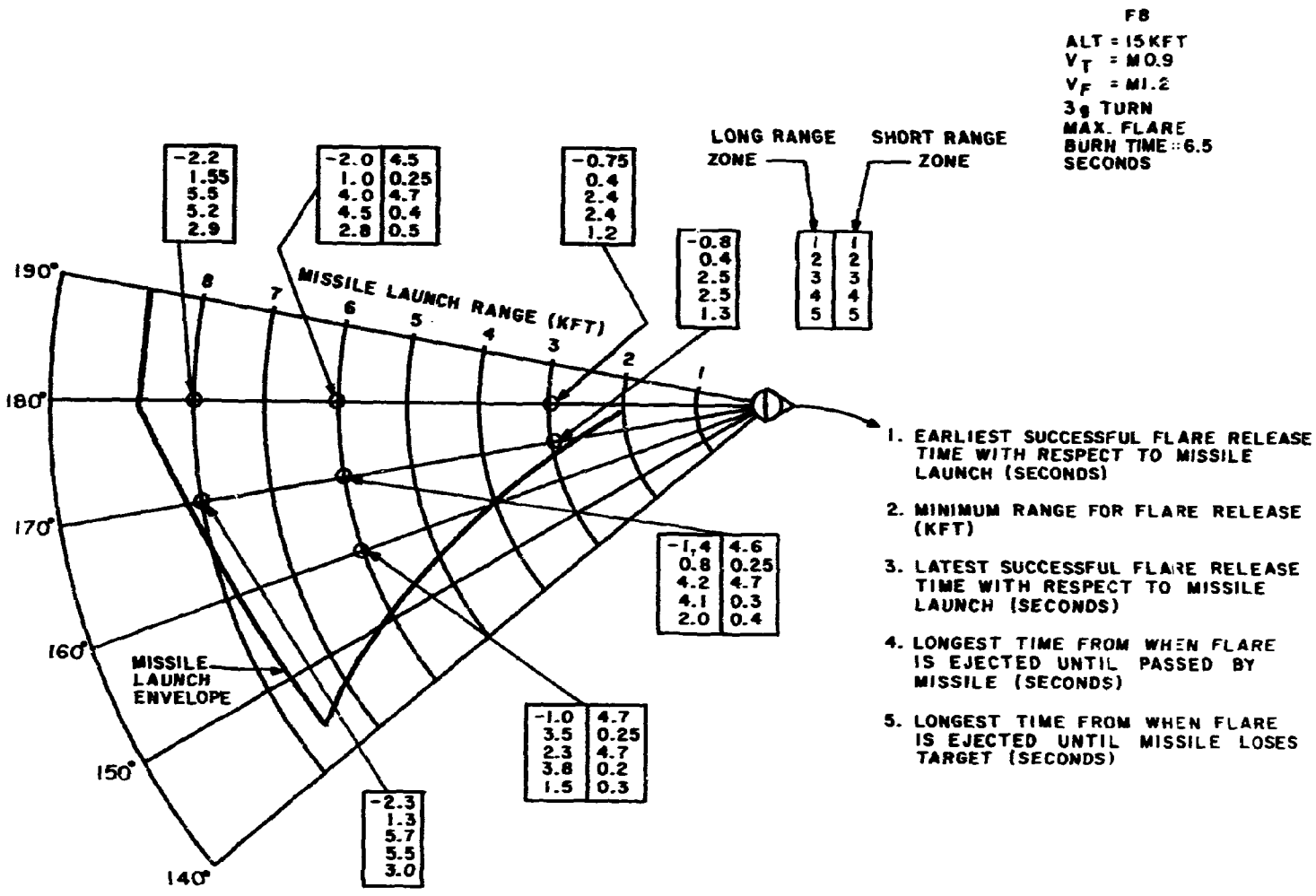


FIG. 51 - FLARE EFFECTIVENESS SUMMARY (S)

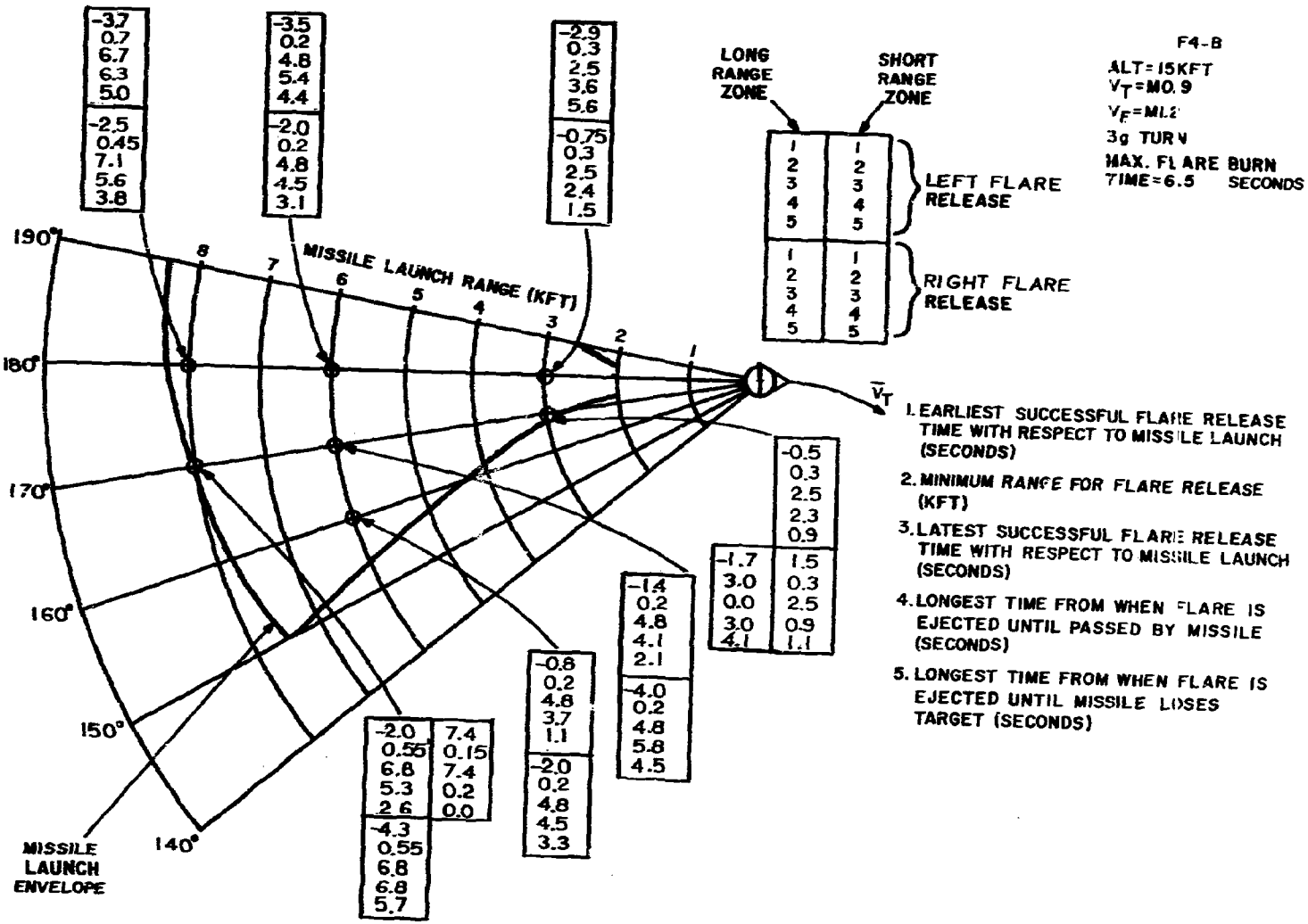


FIG. 52 - FLARE EFFECTIVENESS SUMMARY (S)

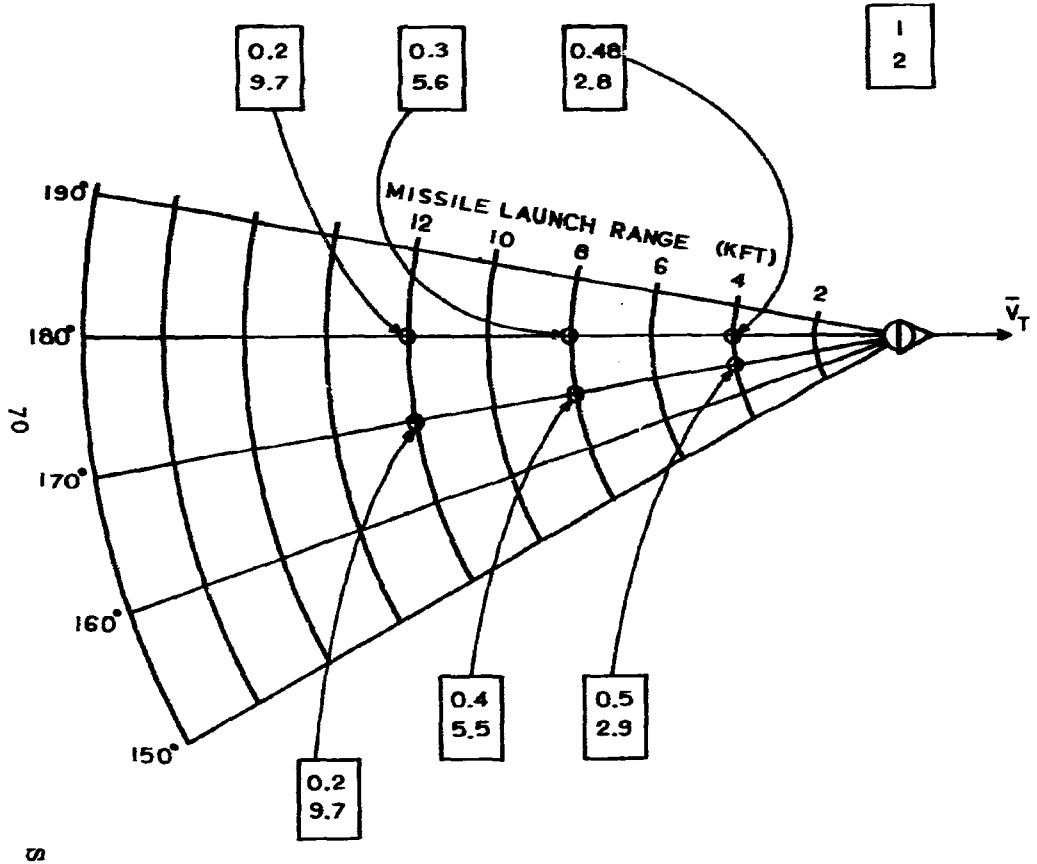


F-8
ALT = 30 KFT
$V_T$ = M0.9
$V_F$ = M1.2
NO MANEUVER
MAX. FLARE BURN
TIME = 8.3 SECONDS

1. MINIMUM RANGE FOR FLARE RELEASE (KFT)
2. LATEST SUCCESSFUL FLARE RELEASE TIME WITH RESPECT TO MISSILE LAUNCH (SECONDS)

FIG. 53 - FLARE EFFECTIVENESS SUMMARY (S)

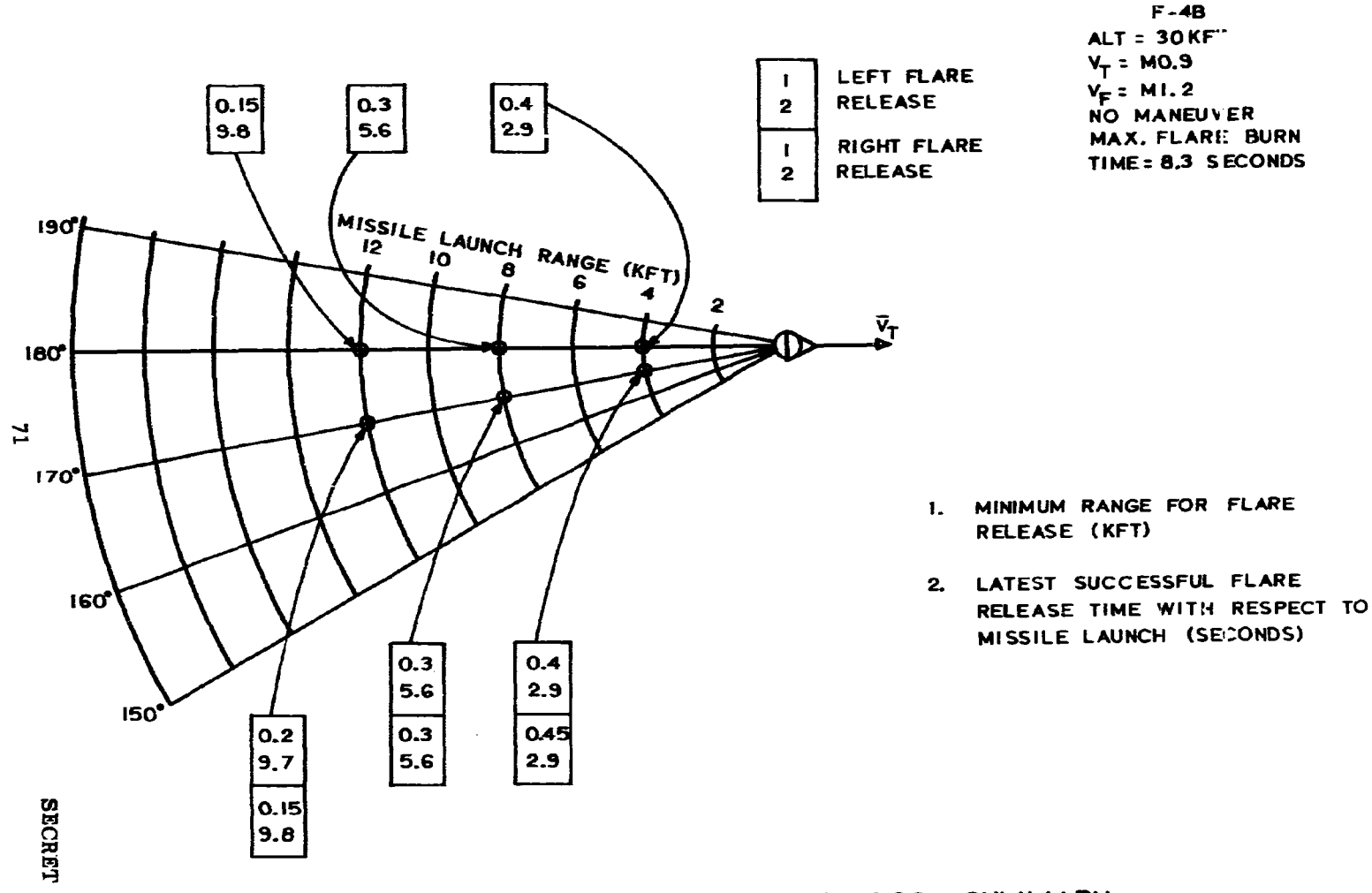


FIG. 54 - FLARE EFFECTIVENESS SUMMARY (S)

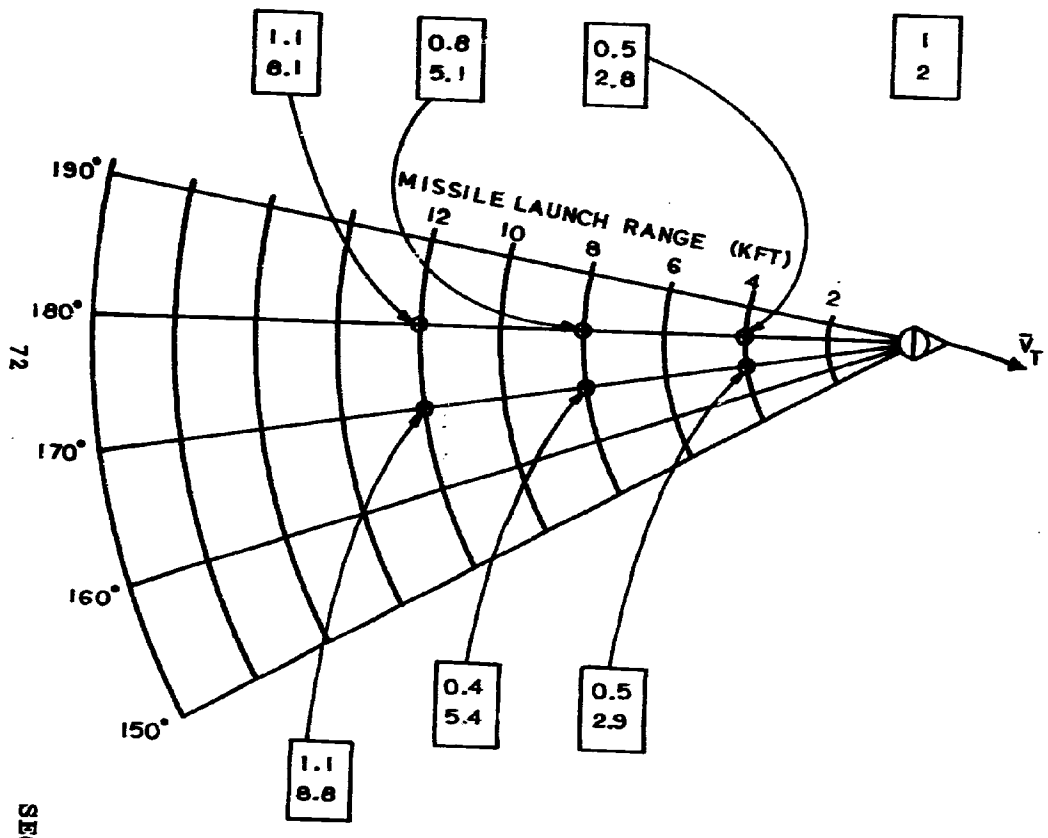


F-8
ALT = 30 KFT
$V_T$ = M0.9
$V_F$ = M1.2
3g TURN
MAX. FLARE BURN
TIME = 8 3 SECONDS

1. MINIMUM RANGE FOR FLARE RELEASE (KFT)
2. LATEST SUCCESSFUL FLARE RELEASE TIME WITH RESPECT TO MISSILE LAUNCH (SECONDS)

72



FIG. 55 - FLARE EFFECTIVENESS SUMMARY (S)

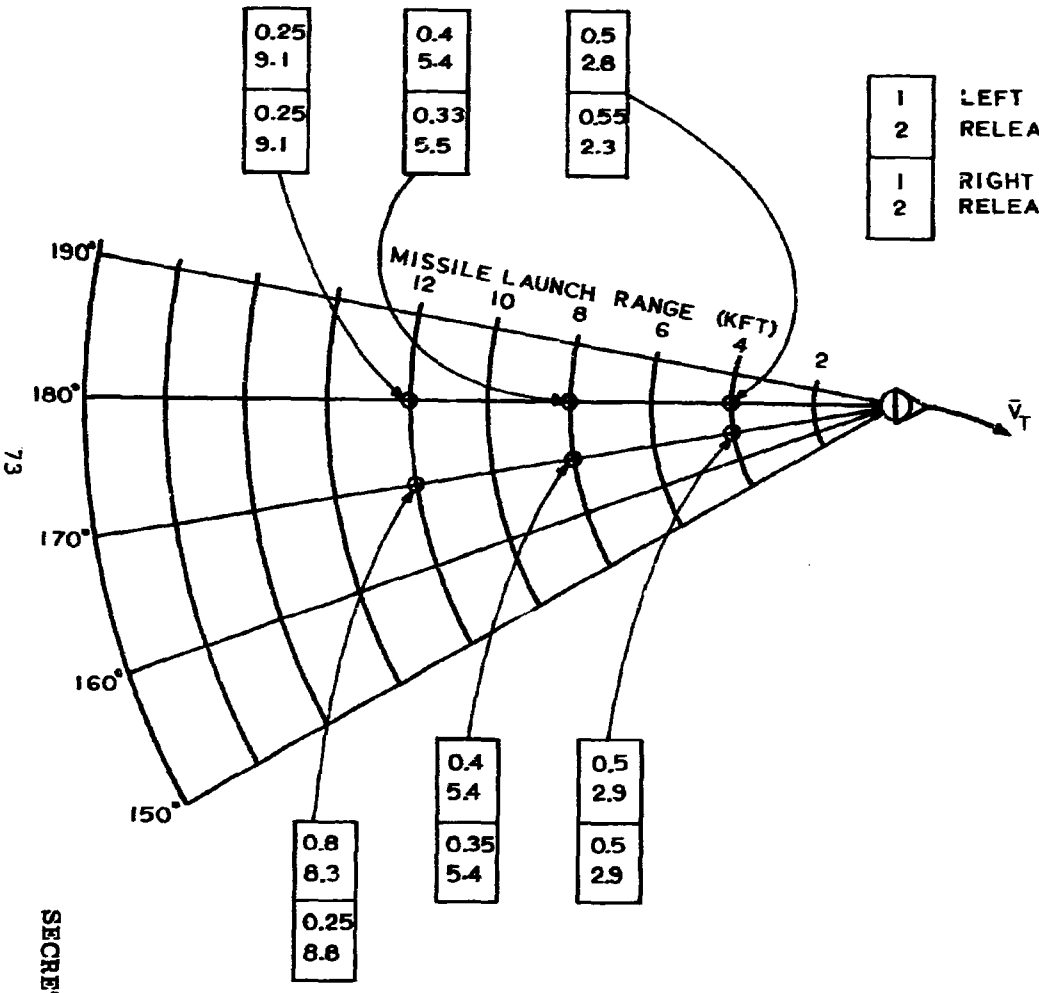


1. MINIMUM RANGE FOR FLARE RELEASE (KFT)
2. LATEST SUCCESSFUL FLARE RELEASE TIME WITH RESPECT TO MISSILE LAUNCH (SECONDS)

FIG. 56 - FLARE EFFECTIVENESS SUMMARY (S)

SECRET-NOFORN
Security Classification

**DOCUMENT CONTROL DATA - R & D**

*(Security classification of title, body of abstract and indexing annotation must be entered when the overall report is classified)*

1. ORIGINATING ACTIVITY *(Corporate author)*
Naval Research Laboratory
Washington, D.C. 20390

2a. REPORT SECURITY CLASSIFICATION
SECRET-NOFORN

2b. GROUP
3

3. REPORT TITLE
F-4B AND F-8 FLARE EFFECTIVENESS AGAINST THE ATOLL MISSILE (AA-2) (U)

4. DESCRIPTIVE NOTES *(Type of report and inclusive dates)*
A final report on one phase of a continuing problem.

5. AUTHOR(S) *(First name, middle initial, last name)*
Harold Toothman and Clair Loughmiller

| 6. REPORT DATE | 7a. TOTAL NO. OF PAGES | 7b. NO. OF REFS |
|---|---|---|
| July 1971 | 80 | 4 |

| 8a. CONTRACT OR GRANT NO. | 9a. ORIGINATOR'S REPORT NUMBER(S) |
|---|---|
| NRL Problem D01-03 | |
| b. PROJECT NO. A05-5333647/652-1/53190000<br>A05-536-318/652-1/W3312-00-00 | NRL Memorandum Report 2297 |
| c. | 9b. OTHER REPORT NO(S) *(Any other numbers that may be assigned this report)* |
| d. | |

10. DISTRIBUTION STATEMENT
Distribution limited to U.S. Government Agencies only; test and evaluation; July 1971. Other requests for this document must be referred to the Director, Naval Research Laboratory, Washington, D.C. 20390.

| 11. SUPPLEMENTARY NOTES | 12. SPONSORING MILITARY ACTIVITY |
|---|---|
| Special handling required; not releasable to foreign nationals. | NAVAIRSYSCOM<br>Department of the Navy<br>Washington, D.C. 20360 |

13. ABSTRACT

(SECRET)

The effectiveness of flares as a countermeasure for the ATOLL missile was investigated for the F-4B and F-8 aircraft. Many different flare ejection times for each value of missile launch range, launch aspect angle, target maneuver, and ejection direction were examined by digital simulation. Although in most cases the flare effectively counters the ATOLL, many cases required that the flare, to be effective, had to be ejected within a narrow time interval.

| 14 KEY WORDS | LINK A | | LINK B | | LINK C | |
|---|---|---|---|---|---|---|
| | ROLE | WT | ROLE | WT | ROLE | WT |
| Flare effectiveness | | | | | | |
| Countermeasures | | | | | | |
| ATOLL missile AA-2 | | | | | | |
| F-4B and F-8 aircraft | | | | | | |

# Naval Research Laboratory
# Technical Library
# Research Reports Section

**DATE:** August 22, 2002

**FROM:** Mary Templeman, Code 5227

**TO:** **Code 5300 Paul Hughes**

**CC:** Tina Smallwood, Code 1221.1 to 8/19/03

**SUBJ:** Review of NRL Reports

Dear Sir/Madam:

Please review NRL Memo Reports 2139,2150,2170,2297,2360,2425,2426 and 2429 for:

- ☑ Possible Distribution Statement
- ☑ Possible Change in Classification

Thank you,

Mary Templeman

Mary Templeman
(202)767-3425
maryt@library.nrl.navy.mil

---

The subject report can be:

- ☑ Changed to Distribution A (Unlimited)
- ☑ Changed to Classification _____
- ☐ Other:

Paul K. Hughes II 8/18/2003

Signature Date

-- 1 OF 1
-- 1 - AD NUMBER: 517147
-- 2 - FIELDS AND GROUPS: 1/3.3, 17/4.4, 19/1.1
-- 3 - ENTRY CLASSIFICATION: UNCLASSIFIED
-- 5 - CORPORATE AUTHOR: NAVAL RESEARCH LAB WASHINGTON D C
-- 6 - UNCLASSIFIED TITLE: F-4B AND F-8 FLARE EFFECTIVENESS AGAINST
-- THE ATOLL MISSILE (AA-2).
-- 8 - TITLE CLASSIFICATION: UNCLASSIFIED
-- 9 - DESCRIPTIVE NOTE: FINAL REPT.,
--10 - PERSONAL AUTHORS: TOOTHMAN,HAROLD ;LOUGHMILLER,CLAIR M. ;
--11 - REPORT DATE: JUL 1971
--12 - PAGINATION: 80P MEDIA COST: $ 7.00 PRICE CODE: AA
--14 - REPORT NUMBER: NRL-MR-2297
--16 - PROJECT NUMBER: A05-536-318/652-1/W3312-00-00, NRL-53D01-03
--20 - REPORT CLASSIFICATION: CONFIDENTIAL
--22 - LIMITATIONS (ALPHA): DISTRIBUTION LIMITED TO U.S. GOV'T.
-- AGENCIES ONLY; TEST AND EVALUATION; JUL 71. OTHER REQUESTS FOR THIS
-- DOCUMENT MUST BE REFERRED TO DIRECTOR, NAVAL RESEARCH LAB.,
-- WASHINGTON, D. C. 20390.
--23 - DESCRIPTORS: (*AIRCRAFT FLARES, AIR TO AIR MISSILES),
-- EFFECTIVENESS, SIMULATION
--24 - DESCRIPTOR CLASSIFICATION: UNCLASSIFIED
--29 - INITIAL INVENTORY: 2

-
--32 - REGRADE CATEGORY: C
--33 - LIMITATION CODES: 3
--34 - SOURCE SERIES: F
--35 - SOURCE CODE: 251950
--36 - ITEM LOCATION: DTIC
--38 - DECLASSIFICATION DATE: OADR
--40 - GEOPOLITICAL CODE: 1100
--41 - TYPE CODE: N
--43 - IAC DOCUMENT TYPE:
--49 - AUTHORITY FOR CHANGE: S TO C GP-3